X-ray Crystal Structures of α-KrF_2, $[KrF][MF_6]$ (M = As, Sb, Bi), $[Kr_2F_3][SbF_6]\cdot KrF_2$, $[Kr_2F_3]_2[SbF_6]_2\cdot KrF_2$, and $[Kr_2F_3][AsF_6]\cdot[KrF][AsF_6]$; Synthesis and Characterization of $[Kr_2F_3][PF_6]\cdot nKrF_2$; and Theoretical Studies of KrF_2, KrF^+, $Kr_2F_3^+$, and the $[KrF][MF_6]$ (M = P, As, Sb, Bi) Ion Pairs†

John F. Lehmann,‡ David A. Dixon,§ and Gary J. Schrobilgen*,‡

Department of Chemistry, McMaster University, Hamilton, Ontario L8S 4M1, Canada, and William R. Wiley Environmental Molecular Sciences Laboratory, Pacific Northwest National Laboratory, 906 Batelle Boulevard, P.O. Box 999, KI-83, Richland, Washington 99352

Received October 23, 2000

The crystal structures of α-KrF_2 and salts containing the KrF^+ and $Kr_2F_3^+$ cations have been investigated for the first time using low-temperature single-crystal X-ray diffraction. The low-temperature α-phase of KrF_2 crystallizes in the tetragonal space group *I*4/*mmm* with $a = 4.1790(6)$ Å, $c = 6.489(1)$ Å, $Z = 2$, $V = 113.32(3)$ Å^3, $R_1 = 0.0231$, and $wR_2 = 0.0534$ at −125 °C. The $[KrF][MF_6]$ (M = As, Sb, Bi) salts are isomorphous and isostructural and crystallize in the monoclinic space group $P2_1/c$ with $Z = 4$. The unit cell parameters are as follows: β-$[KrF][AsF_6]$, $a = 5.1753(2)$ Å, $b = 10.2019(7)$ Å, $c = 10.5763(8)$ Å, $\beta = 95.298(2)°$, $V = 556.02(6)$ Å^3, $R_1 = 0.0265$, and $wR_2 = 0.0652$ at −120 °C; $[KrF][SbF_6]$, $a = 5.2922(6)$ Å, $b = 10.444(1)$ Å, $c = 10.796(1)$ Å, $\beta = 94.693(4)°$, $V = 594.73(1)$ Å^3, $R_1 = 0.0266$, $wR_2 = 0.0526$ at −113 °C; $[KrF][BiF_6]$, $a = 5.336(1)$ Å, $b = 10.513(2)$ Å, $c = 11.046(2)$ Å, $\beta = 94.79(3)°$, $V = 617.6(2)$ Å^3, $R_1 = 0.0344$, and $wR_2 = 0.0912$ at −130 °C. The $Kr_2F_3^+$ cation was investigated in $[Kr_2F_3][SbF_6]\cdot KrF_2$, $[Kr_2F_3]_2[SbF_6]_2\cdot KrF_2$, and $[Kr_2F_3][AsF_6]\cdot[KrF][AsF_6]$. $[Kr_2F_3]_2[SbF_6]_2\cdot KrF_2$ crystallizes in the monoclinic $P2_1/c$ space group with $Z = 4$ and $a = 8.042(2)$ Å, $b = 30.815(6)$ Å, $c = 8.137(2)$ Å, $\beta = 111.945(2)°$, $V = 1870.1(7)$ Å^3, $R_1 = 0.0376$, and $wR_2 = 0.0742$ at −125 °C. $[Kr_2F_3][SbF_6]\cdot KrF_2$ crystallizes in the triclinic $P\bar{1}$ space group with $Z = 2$ and $a = 8.032(3)$ Å, $b = 8.559(4)$ Å, $c = 8.948(4)$ Å, $\alpha = 69.659(9)°$, $\beta = 63.75(1)°$, $\gamma = 82.60(1)°$, $V = 517.1(4)$ Å^3, $R_1 = 0.0402$, and $wR_2 = 0.1039$ at −113 °C. $[Kr_2F_3][AsF_6]\cdot[KrF][AsF_6]$ crystallizes in the monoclinic space group $P2_1/c$ with $Z = 4$ and $a = 6.247(1)$ Å, $b = 24.705(4)$ Å, $c = 8.8616(6)$ Å, $\beta = 90.304(6)°$, $V = 1367.6(3)$ Å^3, $R_1 = 0.0471$ and $wR_2 = 0.0958$ at −120 °C. The terminal Kr−F bond lengths of KrF^+ and $Kr_2F_3^+$ are very similar, exhibiting no crystallographically significant variation in the structures investigated (range, 1.765(3)−1.774(6) Å and 1.780(7)−1.805(5) Å, respectively). The Kr−F bridge bond lengths are significantly longer, with values ranging from 2.089(6) to 2.140(3) Å in the KrF^+ salts and from 2.027(5) to 2.065(4) Å in the $Kr_2F_3^+$ salts. The Kr−F bond lengths of KrF_2 in $[Kr_2F_3][SbF_6]\cdot KrF_2$ and $[Kr_2F_3]_2[SbF_6]_2\cdot KrF_2$ range from 1.868(4) to 1.888(4) Å and are similar to those observed in α-KrF_2 (1.894(5) Å). The synthesis and Raman spectrum of the new salt, $[Kr_2F_3][PF_6]\cdot nKrF_2$, are also reported. Electron structure calculations at the Hartree−Fock and local density-functional theory levels were used to calculate the gas-phase geometries, charges, Mayer bond orders, and Mayer valencies of KrF^+, KrF_2, $Kr_2F_3^+$, and the ion pairs, $[KrF][MF_6]$ (M = P, As, Sb, Bi), and to assign their experimental vibrational frequencies.

Introduction

The known compounds of krypton are limited to the +2 oxidation state and include KrF_2,[1−9] salts of the KrF^+,[10−18] and $Kr_2F_3^+$ [11−13,15,16,18] cations, the molecular adducts $KrF_2\cdot MOF_4$ (M = Cr, Mo, W),[19,20] $KrF_2\cdot nMoOF_4$ ($n = 2, 3$),[19] $KrF_2\cdot VF_5$,[21] and $KrF_2\cdot MnF_4$,[22] the RCN−KrF^+ (R = H, CF_3, C_2F_5, *n*-C_3F_7) cations,[23,24] and $Kr(OTeF_5)_2$.[25] While the strong oxidant characters of KrF_2, KrF^+, and $Kr_2F_3^+$ provide clean, low-temperature synthetic routes to BrF_6^+,[13,26] ClF_6^+,[27] OsO_2F_4,[28] AuF_5,[14] and $TcOF_5$,[29] they have also served as a significant impediment to their detailed structural characterization by single-

† Dedicated to the memory of our colleague and friend, Karel (Drago) Lutar (December 1, 1947−September 2, 2000) in recognition of his many outstanding contributions to the field of inorganic fluorine chemistry.

* To whom correspondence should be addressed.
‡ McMaster University.
§ Pacific Northwest National Laboratory.

(1) Turner, J. J.; Pimental, G. C. *Science* **1963**, *140*, 974.
(2) MacKenzie, D. R. *Science* **1963**, *141*, 1171.
(3) Schreiner, F.; Malm, J. G.; Hindman, J. C. *J. Am. Chem. Soc.* **1965**, *87*, 25.
(4) Streng, L. V.; Streng, A. G. *Inorg. Chem.* **1966**, *5*, 328.
(5) Prusakov, V. N.; Sokolov, V. B. *At. Energy* **1971**, *31*, 259.
(6) Slivnik, J.; Šmalc, A.; Lutar, K.; Žemva, B.; Frlec, B. *J. Fluorine Chem.* **1975**, *5*, 273.
(7) (a) Bezmel'nitsyn, V. N.; Legasov, V. A.; Chaivanov, B. B. *Proc. Acad. Sci. USSR, Chem. Sect.* **1977**, *235*, 365. (b) *Dokl. Akad. Nauk. SSSR* **1977**, *235*, 96.
(8) Šmalc, A.; Lutar, K.; Žemva, B. *Inorg. Synth.* **1992**, *29*, 11.
(9) Kinkead, S. A.; FitzPatrick, J. R.; Foropoulos, J., Jr.; Kissane, R. J.; Purson, J. D. In *Fluorine Chemistry Toward the 21st Century*; Thrasher, J. S., Strauss, S. H., Eds.; ACS Symposium Series 555; American Chemical Society: Washington, DC, 1994; Chapter 3, pp 40−55.
(10) Selig, H.; Peacock, R. D. *J. Am. Chem. Soc.* **1964**, *86*, 5.
(11) Frlec, B.; Holloway, J. H. *J. Chem. Soc., Chem. Commun.* **1973**, 370.
(12) Frlec, B.; Holloway, J. H. *J. Chem. Soc., Chem. Commun.* **1974**, 89.
(13) Gillespie, R. J.; Schrobilgen, G. J. *J. Chem. Soc., Chem. Commun.* **1974**, 90.

10.1021/ic001167w CCC: $20.00
Published on Web 05/22/2001

crystal X-ray diffraction. With the exception of KrF_2, no other krypton compound has been structurally characterized in detail by diffraction techniques. Of the two phases of KrF_2 identified by variable-temperature Raman spectroscopy,[30] only the X-ray crystal structure of the high-temperature β-phase has been reported at −80 °C,[31] although an incorrect determination of the unit cell parameters of the β-phase at room temperature had been reported earlier.[32]

Krypton difluoride has been shown to exhibit fluoride ion donor properties that are analogous to those established for XeF_2.[18,19,33−36] The reaction of KrF_2 with strong fluoride ion acceptors leads to the formation of a number of KrF^+ and $Kr_2F_3^+$ salts, i.e., $[KrF][MF_6]$ (M = As, Sb, Bi, Au, Pt, Ta),[11−17] $[KrF][M_2F_{11}]$ (M = Sb, Ta, Nb),[10,11,13,15,16] and $[Kr_2F_3][MF_6]$ (M = As, Sb, Ta).[11−13,15,16] The physical and spectroscopic properties of these salts have been reviewed by Selig and Holloway.[18] Unlike their xenon(II) analogues, the majority of, if not all, krypton(II) compounds are thermodynamically unstable. The relative kinetic stabilities of their salts, however, show considerable variance.[11−17] A number of salts such as $[KrF][SbF_6]$,[12,13,16] $[KrF][Sb_2F_{11}]$,[10,15,16] $[Kr_2F_3][SbF_6]$,[13,15,16] and $[KrF][AuF_6]$[14] can be handled and stored at room temperature for appreciable periods of time without significant decomposition.

Structural characterization of the KrF^+ and $Kr_2F_3^+$ salts in the solid state using Raman spectroscopy has been most extensive.[11−17] The Raman spectra of KrF^+ salts also indicate that the KrF^+ cation strongly interacts with the anion by formation of a fluorine bridge between krypton and a fluorine of the anion, as is the case for XeF^+ in the crystal structures of $[XeF][AsF_6]$,[35] $[XeF][Sb_2F_{11}]$,[33] and $[XeF][RuF_6]$.[34] Consequently, fluorine bridge modes and vibrational modes resulting from symmetry lowering of the octahedral anion have been reported and tentatively assigned.[14−17] The Raman spectra of $Kr_2F_3^+$ salts have been assigned on the basis of a V-shaped fluorine-bridged geometry for the cation,[13,16] analogous to that established by X-ray crystallography for $Xe_2F_3^+$.[37,38] Unlike the vibrational assignments for $Xe_2F_3^+$,[37,38] the vibrational assignments of $Kr_2F_3^+$ are based on an unsymmetrical cation.[13,15,16] In contrast with the KrF^+ salts, the cation−anion interactions in the $Kr_2F_3^+$ salts appear to be weak, as indicated by retention of octahedral symmetry by the anion. The Lewis acid properties of KrF^+ that lead to fluorine bridging in the salts are further manifested in the formation of adducts with the nitrogen electron pair in oxidatively resistant nitriles to give the adduct cations $RCN{-}KrF^+$ (R = H, CF_3, C_2F_5, n-C_3F_7), which provide the first examples of Kr−N bonds.[23,24] Fluorine-19 NMR spectroscopy has also been used to study the KrF^+ cation in HF solution and the $Kr_2F_3^+$ cation in BrF_5 solution and has provided the first unambiguous characterization of the structure of the fluorine-bridged $Kr_2F_3^+$ cation.[13,16]

The adducts of KrF_2 with weak fluoride ion acceptor metal oxide tetrafluorides, $KrF_2{\cdot}MOF_4$ (M = Mo, W) and $KrF_2{\cdot}n MoOF_4$ (n = 2, 3), have been extensively studied in SO_2ClF solution by low-temperature ^{19}F NMR spectroscopy and have been shown to contain Kr−F_b--M (F_b, bridge fluorine) bridges, which are nonlabile in solution at low temperatures on the NMR time scale.[19] The adducts $KrF_2{\cdot}MOF_4$ (M = Cr, Mo, W)[19,20] and $KrF_2{\cdot}VF_5$ [21] have been studied in the solid state by vibrational spectroscopy. The compounds are consistent with the weaker fluoride ion acceptor properties of MOF_4 and VF_5, and are best represented as covalent adducts in which KrF_2 is weakly fluorine bridged to the transition metal, so that the Kr−F_t (F_t, terminal fluorine) and Kr−F_b bond lengths are expected to be similar to those of free KrF_2. With the exception of $XeF_2{\cdot}CrOF_4$, which is presently unknown, the vibrational spectra[19] and solution ^{19}F and ^{129}Xe NMR spectra[36] of the analogous XeF_2 adducts of $MoOF_4$ and WOF_4 have been reported, and the crystal structure of F−Xe−F--WOF_4 has been determined.[39]

The present study reports the first detailed X-ray crystallographic study of salts containing the KrF^+ and $Kr_2F_3^+$ cations and confirms the dimorphism of KrF_2 by determination of the X-ray structure of the low-temperature phase. Theoretical calculations have been used to arrive at the energy-minimized gas-phase geometries and to reassign or confirm earlier vibrational assignments of KrF_2, the $[KrF][MF_6]$ (M = P, As, Sb, Bi) ion pairs, and $Kr_2F_3^+$ in the gas phase. The effects of crystal packing on the geometries of the $[KrF][MF_6]$ ion pairs and the $Kr_2F_3^+$ cation are also assessed in light of their calculated gas-phase geometries.

Results and Discussion

X-ray Crystal Structures of α-KrF_2 and Salts of the KrF^+ and $Kr_2F_3^+$ Cations. The unit cell parameters and refinement statistics for the title compounds are given in Table 1. Important bond lengths, contacts, and bond angles are listed in Tables 2−4. With the exception of $[Kr_2F_3][AsF_6]{\cdot}[KrF][AsF_6]$, which was refined as a merohedral twin, all of the KrF^+ and $Kr_2F_3^+$ salts were isolated and solved as single crystals.

The $[KrF][MF_6]$ (M = As, Sb, Bi), $[Kr_2F_3][SbF_6]{\cdot}KrF_2$, $[Kr_2F_3]_2[SbF_6]_2{\cdot}KrF_2$, and $[Kr_2F_3][AsF_6]{\cdot}[KrF][AsF_6]$ salts were synthesized by reaction of KrF_2 with MF_5 in 1:1, 1:1, 2:1, 3.5:

(14) Holloway, J. H.; Schrobilgen, G. J. *J. Chem. Soc., Chem. Commun.* **1975**, 623.
(15) Frlec, B.; Holloway, J. H. *Inorg. Chem.* **1976**, *15*, 1263.
(16) Gillespie, R. J.; Schrobilgen, G. J. *Inorg. Chem.* **1976**, *15*, 22.
(17) Gillespie, R. J.; Martin, D.; Schrobilgen, G. J. *J. Chem. Soc., Dalton Trans.* **1980**, 1898.
(18) Selig, H.; Holloway, J. H. In *Topics in Current Chemistry*; Boschke, F. L., Ed.; Springer-Verlag: Berlin, 1984; Vol. 124, pp 33−90.
(19) Holloway, J. H.; Schrobilgen, G. J. *Inorg. Chem.* **1981**, *20*, 3363.
(20) Christe, K. O.; Wilson, W. W.; Bougon, R. A. *Inorg. Chem.* **1986**, *25*, 2163.
(21) Žemva, B.; Slivnik, J.; Šmalc, A. *J. Fluorine Chem.* **1975**, *6*, 191.
(22) Lutar, K.; Jesih, A.; Žemva, B. *Polyhedron* **1988**, *7*, 1217.
(23) Schrobilgen, G. J. *J. Chem. Soc., Chem. Commun.* **1988**, 863.
(24) Schrobilgen, G. J. *J. Chem. Soc., Chem. Commun.* **1988**, 1506.
(25) Sanders, J. C. P.; Schrobilgen, G. J. *J. Chem. Soc., Chem. Commun.* **1989**, 1576.
(26) Gillespie, R. J.; Schrobilgen, G. J. *Inorg. Chem.* **1974**, *13*, 1230.
(27) Christe, K. O.; Wilson, W. W.; Curtis, E. C. *Inorg. Chem.* **1983**, *22*, 3056.
(28) Christe, K. O.; Dixon, D. A.; Mack, H. G.; Oberhammer, H.; Pagelot, A.; Sanders, J. C. P.; Schrobilgen, G. J. *J. Am. Chem. Soc.* **1993**, *115*, 11279.
(29) LeBlond, N.; Mercier, H. P. A.; Dixon, D. A.; Schrobilgen, G. J. *Inorg. Chem.* **2000**, *39*, 4494.
(30) Al-Mukhtar, M.; Holloway, J. H.; Hope, E. G.; Schrobilgen, G. J. *J. Chem. Soc., Dalton Trans.* **1991**, 2831.
(31) Burbank, R. D.; Falconer, W. E.; Sunder, W. A. *Science* **1972**, *178*, 1285.
(32) Siegel, S.; Gebert, E. *J. Am. Chem. Soc.* **1964**, *86*, 3896.
(33) Burgess, J.; Fraser, C. J. W.; McRae, V. M.; Peacock, R. D.; Russell, D. R. In *Herbert H. Hyman Memorial Volume, J. Inorg. Nucl. Chem. Supplement*; Katz, J. J., Sheft, I., Eds.; Pergamon Press: Oxford, 1976; p 183.
(34) Bartlett, N.; Gennis, M.; Gibler, D. D.; Morrell, B. K.; Zalkin, A. *Inorg. Chem.* **1973**, *12*, 1717.
(35) Zalkin, A.; Ward, D. L.; Biagioni, R. N.; Templeton, D. H.; Bartlett, N. *Inorg. Chem.* **1978**, *17*, 1318.
(36) Holloway, J. H.; Schrobilgen, G. J. *Inorg. Chem.* **1980**, *19*, 2632.
(37) Bartlett, N.; DeBoer, B. G.; Hollander, F. J.; Sladky, F. O.; Templeton, D. H.; Zalkin, A. *Inorg. Chem.* **1974**, *13*, 780.
(38) Fir, B. A.; Gerken, M.; Pointner, B. E.; Mercier, H. P. A.; Dixon, D. A.; Schrobilgen, G. J. *J. Fluorine Chem.* **2000**, *105*, 159.
(39) Tucker, P. A.; Taylor, P. A.; Holloway, J. H.; Russell, D. R. *Acta Crystallogr., Sect. B* **1975**, *31*, 906.

Table 1. Summary of Crystal Data and Refinement Results for α-KrF_2, $[KrF][MF_6]$ (M = As, Sb, Bi), $[Kr_2F_3][SbF_6]\cdot KrF_2$, $[Kr_2F_3]_2[SbF_6]_2\cdot KrF_2$, and $[Kr_2F_3][AsF_6]\cdot[KrF][AsF_6]$

	α-KrF_2	β-$[KrF][AsF_6]$	$[KrF][SbF_6]$	$[KrF][BiF_6]$	$[Kr_2F_3]_2[SbF_6]_2\cdot KrF_2$	$[Kr_2F_3][SbF_6]\cdot KrF_2$	$[Kr_2F_3][AsF_6]\cdot[KrF][AsF_6]$
space group	*I*4/*mmm*	$P2_1/c$	$P2_1/c$	$P2_1/c$	$P2_1/c$	$P\bar{1}$	$P2_1/c$
a (Å)	4.1790(6)	5.1753(2)	5.2922(6)	5.336(1)	8.042(2)	8.032(3)	6.247(1)
b (Å)	4.1790(6)	10.2019(7)	10.444(1)	10.513(2)	30.815(6)	8.559(4)	24.705(4)
c (Å)	6.489(1)	10.5763(8)	10.796(1)	11.046(2)	8.137(2)	8.948(4)	8.8616(6)
α (deg)	90	90	90	90	90	69.659(9)	90
β (deg)	90	95.298(2)	94.693(4)	94.79(3)	111.945(3)	63.75(1)	90.304(6)
γ (deg)	90	90	90	90	90	82.60(1)	90
V (Å^3)	113.32(3)	556.02(6)	594.73(1)	617.6(2)	1870.1(7)	517.1(4)	1367.6(3)
Z (molecules/unit cell)	2	4	4	4	4	2	4
mol wt (g mol^{-1})	121.80	291.72	338.55	425.78	1042.47	582.15	705.24
ρ_{calcd} (g cm^{-3})	3.570	3.485	3.781	4.579	3.703	3.739	3.425
T (°C)	−125	−120	−113	−130	−125	−113	−120
μ (mm^{-1})	19.60	14.09	12.09	35.72	14.82	15.54	14.70
final agreement factors[a,b]	$R_1 = 0.0231$ $wR_2 = 0.0534$	$R_1 = 0.0265$ $wR_2 = 0.0652$	$R_1 = 0.0266$ $wR_2 = 0.0526$	$R_1 = 0.0344$ $wR_2 = 0.0912$	$R_1 = 0.0376$ $wR_2 = 0.0742$	$R_1 = 0.0402$ $wR_2 = 0.1039$	$R_1 = 0.0471$ $wR_2 = 0.0958$

[a] $R_1 = \sum||F_o| - |F_c||/\sum|F_o|$ for $I > 2\sigma(I)$. [b] $wR_2 = \sum|(|F_o| - |F_c|)w^{1/2}|/\sum(|F_o|w)$ for $I > 2\sigma(I)$.

Table 2. Experimental and Calculated Bond Lengths (Å) and Bond Angles (deg) for KrF_2

	α-KrF_2[a]	β-KrF_2[b]	KrF_2 (gas)[c]	LDFT	HF
		Bond Lengths (Å)			
Kr−F	1.894(5)	1.89(2)	1.889(10)	1.910	1.822
F- - -F	2.71	2.71			
		Bond Angles (deg)			
F−Kr−F	180	180	180	180	180

[a] This work. [b] From ref 31. [c] From ref 41.

1, and 2:1 molar ratios, respectively, in anhydrous HF solvent. Despite repeated attempts, crystals of $[Kr_2F_3][SbF_6]$ could not be obtained. The stoichiometric mixture, $2KrF_2$:SbF_5, was found to decompose rapidly in HF at temperatures as low as −40 °C, resulting in the growth of crystals of the less soluble $[KrF][SbF_6]$ salt. Attempts to crystallize $[Kr_2F_3][SbF_6]$ using an excess of KrF_2 to account for the decomposition resulted in a mixture of crystalline $[KrF][SbF_6]$ and $[Kr_2F_3]_2[SbF_6]_2\cdot KrF_2$ or $[Kr_2F_3][SbF_6]\cdot KrF_2$. Crystallization of $[Kr_2F_3][AsF_6]$ was also unsuccessful but resulted in the discovery of the new crystalline double salt, $[Kr_2F_3][AsF_6]\cdot[KrF][AsF_6]$.

α-KrF_2. The crystal structure of α-KrF_2 (Figure 1) was determined in order to obtain more precise structural parameters for KrF_2, which are important for comparison with other Kr−F bond lengths, and to establish the structural basis for the dimorphism of KrF_2. The dimorphism of KrF_2 was originally studied by Raman spectroscopy in conjunction with a factor-group analysis. This study indicated that the low-temperature phase, α-KrF_2, is isomorphous with XeF_2, which crystallizes in the tetragonal space group *I*4/*mmm* at room temperature.[40] The present study confirms the dimorphism of KrF_2, the correctness of the earlier vibrational spectroscopic analysis, and the space group assignment. The crystal structure of β-KrF_2 has been previously determined at −80 °C, and the β → α phase transition has been shown by variable-temperature Raman spectroscopy to occur below this temperature.[30] The fact that crystals of β-KrF_2 were initially grown by sublimation at −78 °C in the present study and then cooled to −125 °C for X-ray data collection on the α-phase indicates that the β→α phase transition occurs without serious disruption of the crystal lattice (vide infra).

The crystal packing of α-KrF_2 (Figure 1) is analogous to that of XeF_2.[40] All the KrF_2 molecules in this phase are arranged parallel to each other and to the *c*-axis, with eight molecules centered at the corners of the unit cell and one located in the center of the unit cell. This contrasts with the β-phase in which the KrF_2 molecules are centered on the corners of the unit cell lying in the *ab*-plane are rotated by 45° with respect to the *a*-axis. The central KrF_2 molecule also lies in the *ab*-plane but is perpendicular with respect to the molecular axes of KrF_2 molecules occupying the corner positions.[31] Interconversion of the β- and α-phases occurs without loss of crystallinity by means of a 45° rotation of the molecules occupying the corner sites, such that they align with the *a*-axis of the β-phase and a 45° rotation of the central molecule in the opposite direction such that it also lies parallel to the *a*-axis of the α-phase. As a result, the unit cell axes of the β-phase transform into those of the α-phase as follows: $a \rightarrow c$ and b, $c \rightarrow a$, b or b, a.

The Kr−F bond length in α-KrF_2 is 1.894(5) Å (Table 2) and is in excellent agreement with those determined for β-KrF_2 (1.89(2) Å, −80 °C) by X-ray diffraction[31] and for gaseous KrF_2 by electron diffraction (1.889(10) Å, −40 °C).[41] As observed for β-KrF_2, α-KrF_2 is linear by symmetry. Despite contraction of the unit cell volume for the α-phase (113.32(3) Å^3, −125 °C) relative to that of the β-phase (122.5 Å^3, −80 °C) and reorientation of KrF_2 molecules within the cell, the interatomic F···F distance between collinearly orientated KrF_2 molecules is 2.71 Å in both structures.

β-$[KrF][AsF_6]$, $[KrF][SbF_6]$, and $[KrF][BiF_6]$. The title compounds form an isomorphous and isostructural series (Figure 2) in which the KrF^+ cation strongly interacts with the anion by forming a fluorine bridge with the pseudo-octahedral anion that is bent about F_b. The $[KrF][MF_6]$ ion pairs pack in columns along the *a*-axis of the unit cell and are orientated such that alternating cation and anion planes are parallel to the *b*−*c* face (Figure 2d). The point group symmetries of the $[KrF][MF_6]$ ion pairs are C_1 because the F_b--Kr−F_t group is skewed with respect to a plane defined by the axial fluorine (F_a) trans to the bridging fluorine (F_b) and two equatorial fluorines (F_e) trans to each other. The smallest F_e-M- -F_b- -Kr dihedral angles are 22.1, 22.2, 19.7, and 28.1° for β-$[KrF][AsF_6]$, $[KrF][SbF_6]$, $[KrF][BiF_6]$, and $[Kr_2F_3][AsF_6]\cdot[KrF][AsF_6]$, respectively.

As inferred from the Raman spectra, the Kr−F_t bond lengths (1.765(3)−1.774(6) Å) in these salts are significantly shorter, and the Kr- -F_b bridge bond lengths are significantly longer than the Kr−F bonds of α-KrF_2 (1.894(5) Å). The MF_6^- octahedra

(40) Agron, P. A.; Begun, G. M.; Levy, H. A.; Mason, A. A.; Jones, C. G.; Smith, D. F. *Science* **1963**, *139*, 842.

(41) Harshberger, W.; Bohn, R. K.; Bauer, S. H. *J. Am. Chem. Soc.* **1967**, *89*, 6466.

Table 3. Experimental and Calculated Bond Lengths (Å) and Bond Angles (deg) in [KrF][MF_6] (M = As, Sb, Bi) and Calculated Bond Lengths (Å) and Bond Angles (deg) in [KrF][MF_6]

	β-[KrF][AsF_6]			[Kr_2F_3][AsF_6]·[KrF][AsF_6][a]	[KrF][SbF_6]			[KrF][BiF_6]			[KrF][PF_6]	
	exp	LDFT	HF	exp	exp	LDFT	HF	exp	LDFT	HF	LDFT	HF
					Bond Lengths (Å)							
Kr−F(1)	1.765(2)	1.867	1.746	1.783(6)	1.765(3)	1.857	1.739	1.774(6)	1.859	1.745	1.877	1.789
Kr- - -F(2)	2.131(2)	1.998	2.002	2.106(6)	2.140(3)	2.017	2.038	2.090(6)	2.012	2.003	1.972	1.873
M- -F(2)	1.845(2)	2.096	1.972	1.878(6)	1.963(3)	2.185	2.049	2.106(6)	2.266	2.194	2.176	2.493
M−F(3)	1.691(2)	1.709	1.659	1.686(6)	1.856(3)	1.898	1.813	1.944(6)	1.948	1.950	1.561	1.526
M−F(4)	1.698(2)	1.729	1.672	1.711(6)	1.847(3)	1.907	1.821	1.957(6)	1.977	1.969	1.588	1.533
M−F(5)	1.710(2)	1.752	1.700	1.684(7)	1.859(3)	1.907	1.821	1.962(6)	1.977	1.969	1.609	1.572
M−F(6)	1.703(2)	1.734	1.681	1.720(6)	1.861(3)	1.925	1.841	1.938(6)	1.957	1.958	1.592	1.556
M−F(7)	1.703(2)	1.734	1.681	1.685(7)	1.857(3)	1.925	1.841	1.941(6)	1.957	1.958	1.592	1.556
					Bond Angles (deg)							
F(1)−Kr- -F(2)	176.8(1)	177.7	178.3	177.3(3)	177.9(2)	177.4	178.6	177.0(4)	177.2	178.7	178.3	179.3
Kr- -F(2)−M	133.7(1)	120.0	128.3	124.6(3)	139.2(2)	114.1	124.9	138.3(3)	113.8	131.2	119.1	117.2

[a] The fluorine atom labels F(4), F(5), F(6), F(7), F(8), F(9), and F(10) for the [KrF][AsF_6] unit in [Kr_2F_3][AsF_6]·[KrF][AsF_6] (see Figure 5) are given as F(1), F(2), F(3), F(4), F(5), F(6), and F(7), respectively, in this table.

Table 4. Experimental Bond Lengths (Å) and Bond Angles (deg) for the $Kr_2F_3^+$ Cation and MF_6^- (M = As, Sb) Anion in [Kr_2F_3][SbF_6]·KrF_2, [Kr_2F_3]$_2$[SbF_6]$_2$·KrF_2, and [Kr_2F_3][AsF_6]·[KrF][AsF_6] and Calculated Bond Lengths (Å) and Bond Angles (deg) in $Kr_2F_3^+$

	exp			$Kr_2F_3^+$	
	[Kr_2F_3]$_2$[SbF_6]$_2$·KrF_2	[Kr_2F_3][SbF_6]·KrF_2	[Kr_2F_3][AsF_6]·[KrF][AsF_6]	LDFT (C_{2v})	HF ($D_{\infty h}$)
		Bond Lengths (Å)			
Kr(1)−F(1)	1.805(5)	1.800(5)	1.780(7)	1.826	1.730
Kr(2)−F(2)	1.799(4)	1.790(5)	1.803(6)	1.826	1.730
Kr(1)- - -F(3)	2.041(4)	2.027(5)	2.061(6)	2.081	2.082
Kr(2)- - -F(3)	2.065(4)	2.046(5)	2.049(6)	2.081	2.082
Kr(3)−F(4)	1.797(5)				
Kr(4)−F(5)	1.787(4)				
Kr(3)- - -F(6)	2.052(5)				
Kr(4)- - -F(6)	2.056(4)				
Kr(5)−F(7)	1.881(4)	1.868(4)			
Kr(5)−F(8)	1.887(4)	1.888(4)			
M−F(9)	1.872(4)	1.875(4)			
M−F(10)	1.880(4)	1.874(4)			
M−F(11)	1.876(4)	1.872(4)	1.689(7)		
M−F(12)	1.879(4)	1.861(4)	1.701(7)		
M−F(13)	1.873(4)	1.875(4)	1.719(7)		
M−F(14)	1.872(4)	1.886(4)	1.710(8)		
M−F(15)	1.882(4)		1.674(9)		
M−F(16)	1.874(4)		1.712(6)		
M−F(17)	1.882(4)				
M−F(18)	1.876(4)				
M−F(19)	1.879(4)				
M−F(20)	1.872(4)				
M−F_6 (mean)	1.876(4)	1.874(8)	1.701(17)		
		Bond Angles (deg)			
F(1)−Kr(1)- - -F(3)	177.9(2)	175.1(2)	178.2(3)	177.4	180.0
F(2)−Kr(2)- - -F(3)	177.8(2)	176.8(2)	178.6(3)	177.4	180.0
F(4)−Kr(3)- - -F(6)	178.7(2)				
F(5)−Kr(4)- - -F(6)	178.3(2)				
Kr(1)- - -F(3)- - -Kr(2)	126.0(2)	142.5(3)	127.5(3)	135.2	180.0
Kr(3)- - -F(6)- - -Kr(4)	128.0(2)				
F(7)−Kr(5)−F(8)	179.1(2)	178.0(2)			

are distorted and have local C_{4v} symmetries that result from strong bridging to the cation, giving rise to a long M- -F_b bond. There is no clear distinction between the M−F_e and the M−F_a bond lengths in these compounds. Despite the strong fluorine bridge interactions and variations in the fluoride ion acceptor strengths of AsF_5, SbF_5, and BiF_5, the Kr−F_t bond lengths in all three salts and the Kr- -F_b bond distances in β-[KrF][AsF_6] (2.131(2) Å) and [KrF][SbF_6] (2.140(3) Å) exhibit no crystallographically significant variation at the 3σ limit. The Kr- -F_b bridge bond length is, however, significantly shorter in the BiF_6^- salt (2.089(6) Å) than in the arsenic and antimony analogues, which is consistent with a weaker fluoride acceptor strength for BiF_5 when compared with those of AsF_5 and SbF_5. Comparison of the Xe- -F_b bonds in β-[XeF_3][SbF_6][42] and [XeF_3][BiF_6][43] reveals the same trend. The Kr- -F_b bond distances of all three salts are significantly less than the sum of the fluorine (1.47, 1.35 Å)[44,45] and krypton (2.02 Å)[44] van der Waals radii and are indicative of significant covalent bond character that is also reflected in the nonlinearity of the Kr- -F_b-M bridge angles (vide infra).

(42) Boldrini, P.; Gillespie, R. J.; Ireland, P. R.; Schrobilgen, G. J. *Inorg. Chem.* **1974**, *13*, 1690.
(43) Gillespie, R. J.; Martin, D.; Schrobilgen, G. J.; Slim, D. R. *J. Chem. Soc., Dalton Trans.* **1977**, 2234.
(44) Bondi, A. *J. Phys. Chem.* **1964**, *68*, 441.
(45) Pauling, L. *The Nature of the Chemical Bond*, 3rd ed.; Cornell University Press: Ithaca, NY, 1960; p 260.

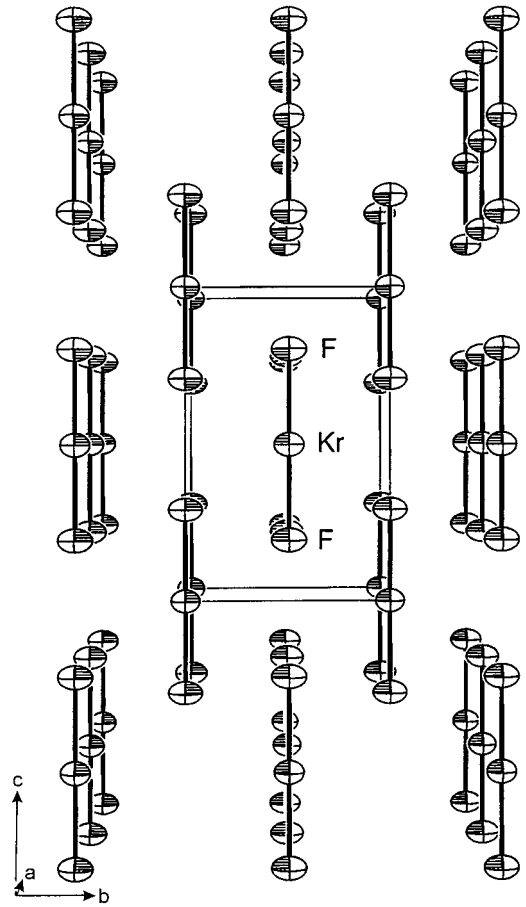

Figure 1. Packing diagram of α-KrF_2 along the *a*-axis.

Variable-temperature Raman spectroscopy has previously shown that [KrF][AsF_6] exhibits a phase transition between 25 and −78 °C. It was expected that [KrF][SbF_6] and the low-temperature β-phase of [KrF][AsF_6] would prove to be isomorphous and isostructural because their similar Raman spectra exhibit the same split ν(Kr−F_t) (615, 619 cm^{-1}) and ν(Kr- -F_b) (338 cm^{-1}) stretching frequencies.[16] The structural relationship has now been verified by the crystal structures of these compounds and their near identical Kr−F_t and Kr- -F_b bond lengths. Although significant lengthening of the Kr−F_t bond with respect to the arsenic and antimony compounds is not observed in the [KrF][BiF_6] structure, the split Kr−F_t stretching frequency is shifted to lower frequency (604, 610 cm^{-1}) and is consistent with a shortening of the Kr- -F_b bond length relative to those in the arsenic and antimony compounds. The effect on the Kr- -F_b stretch cannot be directly assessed for [KrF][BiF_6] because the experimental frequency of this vibration has not been reported; however, the frequency of this mode has been calculated (see Computational Results) and is predicted to have a value similar to that predicted for [KrF][AsF_6]. The splitting of the Kr−F_t stretch in all three compounds[16,17] is now readily understood in terms of their crystal structures and arises from vibrational coupling among the four equivalent structural units in each of their unit cells. A factor-group analysis correlates the C_1 symmetry of the four free ion pairs to their site symmetry, C_1. Correlation of the C_1 site symmetry to the unit cell symmetry, C_{2h}, reveals that each vibrational mode is split into two Raman-active components having A_g and B_g symmetries and into two infrared-active components having A_u and B_u symmetries.[46−48]

Minor deviations from the linear $AXYE_3$ (A = Kr, X = F_t, Y = F_b, E = valence electron lone-pair domain) geometry, predicted by the VSEPR model of molecular geometry,[49] were observed for the F_t-Kr- -F_b bond angle, which ranged from 176.8(1) to 177.9(2)° in the three KrF^+ salts. Similar deviations from linearity are also obtained for the energy-minimized gas-phase geometries (see Computational Results), and therefore cannot be attributed to packing effects alone. The Kr- -F_b- -M bridge bond angles, which also exhibit minor variations over the series β-[KrF][AsF_6] (133.7(1)°), [KrF][SbF_6] (139.2(2)°), and [KrF][BiF_6] (138.3(3)°), are consistent with the bent geometry predicted for an $AXYE_2$ (A = F_b, X = Kr, Y = M) VSEPR arrangement. The angles are considerably more open than the ideal tetrahedral angle owing to the high ionic character of the Kr- -F_b bond.

The structure of the [KrF][AsF_6] ion pair in [Kr_2F_3][AsF_6]·[KrF][AsF_6] differs from that of β-[KrF][AsF_6] in that the dihedral F_e-M- -F_b- -Kr angle (28.1°) in the double salt is larger than that of β-[KrF][AsF_6] (22.1°) and indicates that the geometry of the ion pair is significantly influenced by the crystal packing. The Kr- -F_b bond length is significantly shorter (2.106(6) Å) than in β-[KrF][AsF_6], while the Kr−F_t bond length (1.783(6) Å) shows no significant change.

The effects of secondary Kr···F contacts on the structures of [KrF][MF_6] (M = As, Sb, Bi) and [Kr_2F_3][AsF_6]·[KrF][AsF_6] are difficult to assess. Each isomorphous [KrF][MF_6] structure has eight secondary intermolecular Kr···F contacts (2.980−3.480 Å) that are less than or equal to the sum of the krypton and fluorine van der Waals radii, while the krypton atom of KrF^+ in [Kr_2F_3][AsF_6]·[KrF][AsF_6] has seven such contacts (3.076−3.489 Å). Intramolecular contacts between krypton and an equatorial fluorine in the anion of the same ion pair are only observed in [KrF][AsF_6] (3.301 Å) and [Kr_2F_3][AsF_6]·[KrF][AsF_6] (3.061, 3.449 Å).

[Kr_2F_3]$_2$[SbF_6]$_2$·KrF_2, [Kr_2F_3][SbF_6]·KrF_2, and [Kr_2F_3][AsF_6]·[KrF][AsF_6]. The X-ray crystal structures of the title compounds, along with their packing diagrams, are depicted in Figures 3−5. When viewed along the *a*-axis, the crystal packing of [Kr_2F_3][SbF_6]·KrF_2 consists of alternating cation and equally populated anion/KrF_2 layers (Figure 3b). Columns of $Kr_2F_3^+$ cations run parallel to the *a*-axis with the cations eclipsing each other when viewed along this axis. Columns of alternating SbF_6^- anions and KrF_2 molecules are also observed along the *a*-axis; however, the KrF_2 molecules are off center with respect to the anions.

The packing of [Kr_2F_3]$_2$[SbF_6]$_2$·KrF_2 (Figure 4b) is significantly more complex than that of [Kr_2F_3][SbF_6]·KrF_2. When viewed along the *c*-axis, a layered structure is not evident; however, a complex system of columns can be identified. Half of the $Kr_2F_3^+$ cations form columns in which the cations eclipse one another, while the other half is shifted off center and alternates with the SbF_6^- anions of an adjacent column, which also runs parallel to the *c*-axis. The remaining anions and KrF_2 molecules are arranged in columns in which the KrF_2 molecules are off center with respect to the anion, similar to that observed in [Kr_2F_3][SbF_6]·KrF_2. When viewed along the *a*-axis, there is also no apparent layering, and the view is similar to that observed along the *c*-axis.

Of the solid-state structures investigated in this study, only

(46) Bhagavantam, S.; Venkatarayudu, R. *Proc. Indian Acad. Sci.* **1939**, *9A*, 224.
(47) Carter, R. L. *J. Chem. Educ.* **1971**, *48*, 297.
(48) Fateley, W. G.; Dollish, F. R.; McDevitt, N. T.; Bentley, F. F. *Infrared and Raman Selection Rules for Molecular and Lattice Vibrations: The Correlation Method*; Wiley: New York, 1972.
(49) Gillespie, R. J.; Hargittai, I. *The VSEPR Model of Molecular Geometry*; Allyn and Bacon: Boston 1991.

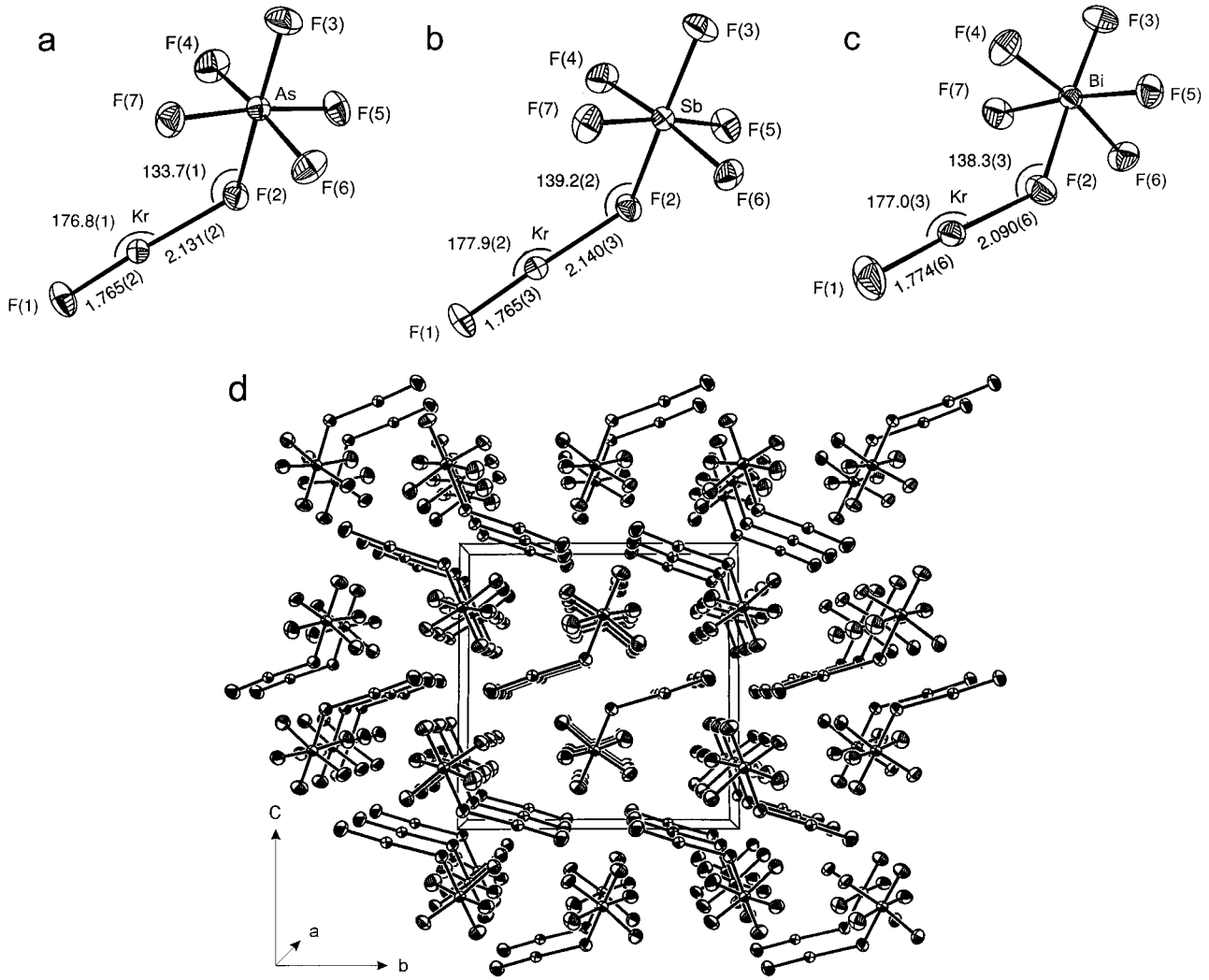

Figure 2. Structures of (a) [KrF][AsF_6], (b) [KrF][SbF_6], (c) [KrF][BiF_6], and (d) packing diagram viewed along the *a*-axis showing the head to tail arrangement of the isomorphous ion pairs, [KrF][MF_6] (M = As, Sb, Bi); thermal ellipsoids are shown at the 50% probability level.

[Kr_2F_3][AsF_6]·[KrF][AsF_6] exhibited crystal twinning. Twinning in this structure is not surprising because of its nearly orthorhombic unit cell (β = 90.304(6)°), which can allow a 90° reorientation of the crystal growth along the *b*-axis. The refined structure was found to contain a 0.489:0.511 population ratio for the two orientations. When viewed along the *a*-axis (Figure 5b), eclipsed columns of $Kr_2F_3^+$, AsF_6^-, and [KrF][AsF_6] are observed. Double layers of [KrF][AsF_6] alternate with double layers of [Kr_2F_3][AsF_6] parallel to the *ac*-plane.

The Kr−F_t bond lengths of the $Kr_2F_3^+$ cations exhibit no crystallographically significant variation among the structures of [Kr_2F_3]$_2$[SbF_6]$_2$·KrF_2 (Figure 3a), [Kr_2F_3][SbF_6]·KrF_2 (Figure 4a), and [Kr_2F_3][AsF_6]·[KrF][AsF_6] (Figure 5a), ranging from 1.780(7) to 1.805(5) Å with an average value of 1.796(9) Å. The longer and more polar Kr- -F_b bonds are somewhat more sensitive to their environments and range from 2.027(5) to 2.065(4) Å with an average value of 2.048(14) Å. Long Kr···F interionic contacts are likely responsible for the variability of Kr- -F_b bond lengths and Kr- -F_b- -Kr bond angles in the structures that have been studied. Half of the $Kr_2F_3^+$ cations in [Kr_2F_3]$_2$[SbF_6]$_2$·KrF_2 are asymmetrical and exhibit a small, but significant, bond length difference between Kr(1)−F_b(3) (2.041(4) Å) and Kr(2)−F_b(3) (2.065(4) Å). This is the first example of an asymmetric $Ng_2F_3^+$ (Ng = Kr, Xe) cation that has been documented crystallographically, although the possibility of an asymmetric $Kr_2F_3^+$ cation in [Kr_2F_3][SbF_6] had been previously proposed on the basis of Raman spectroscopic evidence.[13,15,16] In all other cases, $Ng_2F_3^+$ cations have been described as symmetrical, having C_{2v} point group symmetries.

The F_t-Kr- -F_b bond angles of the $Kr_2F_3^+$ cation structures investigated exhibit small, but significant, distortions from the expected linear $AXYE_3$ VSEPR arrangements, ranging from 177.8(2) to 178.7(2)° in [Kr_2F_3]$_2$[SbF_6]$_2$·KrF_2, from 175.1(2) to 176.8(2)° in [Kr_2F_3][SbF_6]·KrF_2, and from 178.2(3) to 178.6(3)° in [Kr_2F_3][AsF_6]·[KrF][AsF_6]. The most significant bond angle variation occurs for the Kr- -F_b- -Kr bridge, which is 126.0(2) to 128.0(2)° in [Kr_2F_3]$_2$[SbF_6]$_2$·KrF_2, 127.5(3)° in [Kr_2F_3][AsF_6]·[KrF][AsF_6], and largest in [Kr_2F_3][SbF_6]·KrF_2 (142.5(3)°). The variability of the Kr- -F_b- -Kr bond angles of $Kr_2F_3^+$ in these salts can be attributed to long interionic/intermolecular Kr···F contacts[50] and to the effects of crystal packing on these highly deformable angles. In contrast, the small

(50) The effects of secondary contacts on the geometries of the $Kr_2F_3^+$ cations are difficult to assess. The number of Kr···F contacts to the $Kr_2F_3^+$ cations range from 6 to 8 per krypton atom with Kr···F contact distances ranging from 2.902 to 3.489 Å. There are also 6−8 long Kr···F contacts for the adducted KrF_2 molecules, and they vary from 3.104 to 3.473 Å. Of the 58 ($Kr_2F_3^+$) and 14 (KrF_2) Kr···F contacts observed in the structures of [Kr_2F_3][SbF_6]·KrF_2, [Kr_2F_3]$_2$[SbF_6]$_2$·KrF_2, and [Kr_2F_3][AsF_6]·[KrF][AsF_6], 50 ($Kr_2F_3^+$) and 12 (KrF_2) contacts have F_t−Kr···F angles falling in the ranges 52−80° and 100−122°, while the remaining long contact angles fall between 80 and 100°. The angular distribution of long contacts is generally consistent with avoidance of the three valence lone pair domains of krypton.

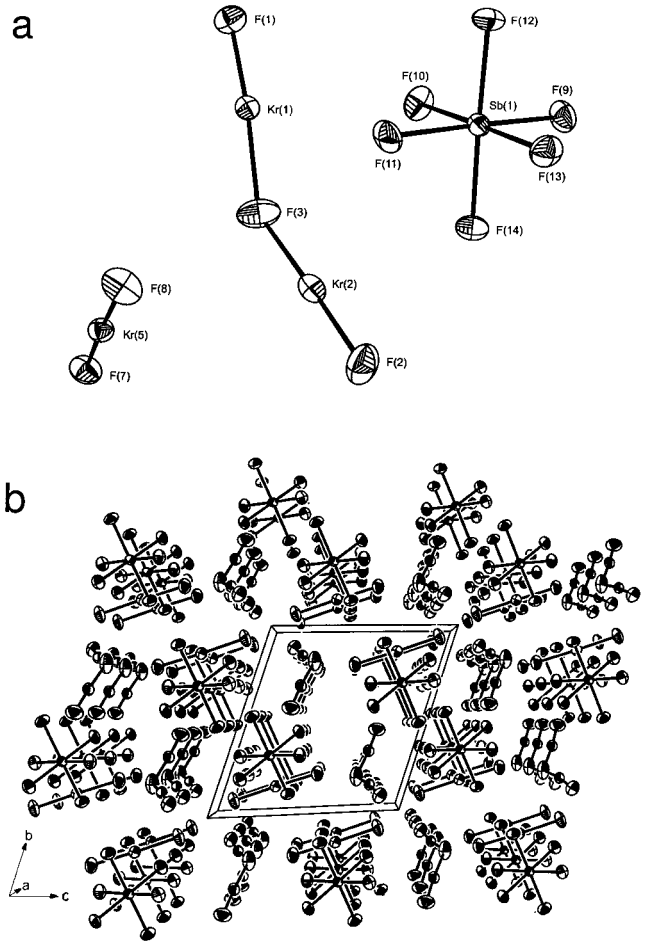

Figure 3. (a) Structure of $[Kr_2F_3][SbF_6]\cdot KrF_2$ and (b) view of the $[Kr_2F_3][SbF_6]\cdot KrF_2$ unit cell along the *a*-axis; thermal ellipsoids are shown at the 50% probability level.

F_t-Kr- -F_b angle distortions that give rise to the W-shaped $Kr_2F_3^+$ cations in these salts are not attributed to secondary Kr···F contacts and crystal packing because they persist in the gas-phase energy-minimized geometry (see Computational Results).

Unlike the KrF_2 molecules in α-KrF_2 and β-KrF_2, which are linear by symmetry, the KrF_2 molecules in $[Kr_2F_3][SbF_6]\cdot KrF_2$ and $[Kr_2F_3]_2[SbF_6]_2\cdot KrF_2$ are slightly bent (178.0(2) and 179.1(2)°) with Kr−F bond lengths of 1.868(4), 1.888(4) Å and 1.881(4), 1.887(4) Å, respectively. The small bond length differences and angle distortions are likely attributable to long Kr···F contacts[50] and to crystal packing, and do not persist in the gas-phase energy-minimized geometry (see Computational Results). The X-ray structure determinations of $[Kr_2F_3]_2[SbF_6]_2\cdot KrF_2$ and $[Kr_2F_3][SbF_6]\cdot KrF_2$ confirm earlier Raman spectroscopic studies of the KrF_2/SbF_5 and KrF_2/AsF_5 systems in which an undetermined excess of KrF_2 was shown to associate with $[Kr_2F_3][SbF_6]$ and $[Kr_2F_3][AsF_6]$.[13,15,16] The symmetric stretch of the associated KrF_2 was shifted to higher frequency of that of free KrF_2 by $\sim$10 cm^{-1} in these studies.

Structural Comparisons Among NgF_2, NgF^+, and $Ng_2F_3^+$ (Ng = Kr, Xe). Experimental trends in bond lengths and bond angles among $[NgF][MF_6]$ ion pairs, NgF_2, and $Ng_2F_3^+$ salts are analogous for krypton and xenon. The Kr−F_t bond exhibits a considerable variation in length among the solid-state krypton fluoride structures that are now known. The Kr−F_t bonds in the KrF^+ salts (1.765(3)−1.783(6) Å) and in the $Kr_2F_3^+$ salts (1.780(7)−1.805(5) Å) show no crystallographically significant differences and are longest in KrF_2 (1.868(4)−1.889(10) Å). This trend is consistent with the valence bond (Structures I−III)- and 3c−4e descriptions of KrF_2, which predict formal Kr−F

$$\underset{\text{I}}{\text{F-Kr}^+\ \text{F}^-} \leftrightarrow \underset{\text{II}}{\text{F-Kr-F}} \leftrightarrow \underset{\text{III}}{\text{F}^-\ \text{Kr-F}^+}$$

bond orders of one-half for KrF_2 and one for the free KrF^+ cation. The Kr−F_t bond length in $Kr_2F_3^+$ is expected to be intermediate with respect to those of KrF_2 and KrF^+ and consistent with the dominant roles KrF^+ and KrF_2 play in the resonance description of $Kr_2F_3^+$ (Structures IV−VI) and with

$$\underset{\text{IV}}{\text{F-Kr-F}\ \text{Kr-F}^+} \leftrightarrow \underset{\text{V}}{\text{F-Kr}^+\ \text{F}^-\ {}^+\text{Kr-F}} \leftrightarrow \underset{\text{VI}}{\text{Kr-F}^+\ \text{F-Kr-F}}$$

a description that invokes a significant contribution from the fully ionic resonance Structure V. Moreover, the Kr- -F_b bond (2.027(5)−2.065(4) Å), though significantly longer than that of KrF_2, has substantial covalent character and is ca. 1.4 Å shorter than the sum of the krypton and fluorine van der Waals radii. The covalency of the Kr- -F_b bond is also reflected in the Kr- -F_b- -Kr bridge angles, which are significantly bent in all three crystal structures containing the $Kr_2F_3^+$ cation. The bent angles are consistent with AX_2E_2 VSEPR arrangements at their respective fluorine bridge atoms but are more open than the ideal tetrahedral angle. The upper limit of the Kr- -F_b- -Kr bond angle (range, 126.0(2)−142.4(3)°) is in good agreement with the Xe- -F_b- -Xe bond angles observed in the monoclinic (148.6(4)°)[37,38] and trigonal (139.8(8)°)[38] phases of $[Xe_2F_3][AsF_6]$ but is considerably smaller than the angle observed in $[Xe_2F_3][SbF_6]$ (160.3(3)°).[38] The X-ray crystal structures and energy-minimized structures derived from electron structure calculations for the $Xe_2F_3^+$ cation [38] and the $Kr_2F_3^+$ cation in this work show that they are W-shaped (see Computational Results), with the F_t-Xe- -F_b angles distorted from linearity by similar amounts (experimental, 2.4(3)° [As] and 1.4(4)° [Sb]; theoretical, 2.3°) when compared with those of $Kr_2F_3^+$ (experimental, 3.2(1)−2.1(2)°; theoretical, 2.6°).

Although the crystal structures of the related XeF^+ salts are not as precise as those determined for the KrF^+ salts described in the present study, the trends in geometrical parameters are clearly analogous. The Xe−F_t bond lengths in the XeF^+ salts of AsF_6^-, $Sb_2F_{11}^-$, and RuF_6^- are 1.873(6), 1.82(3), and 1.87(2) Å, and the Xe- -F_b bond lengths are 2.212(5), 2.34(3), and 2.18(2) Å, respectively.[33−35] At the 3σ limit, the Xe−F_t and Xe- -F_b bond lengths, like their counterparts in $[KrF][MF_6]$, exhibit no crystallographically significant dependence on the counteranion. The F_t-Ng- -F_b angles in both series of salts are very close to linear. Although the distortions from linearity are significant in the krypton series, the uncertainties are too high in the xenon structures to differentiate. The Ng- -F_b- -M angles in both series are significantly bent and are consistent with $AXYE_2$ VSEPR arrangements at their respective fluorine bridge atoms, which, because of the high ionic characters of these bonds, are significantly more open than the ideal tetrahedral angle. The Xe- -F_b- -M angles in the XeF^+ salts, 137.2(5) (RuF_6^-)[34] and 134.8(2)° (AsF_6^-),[35] are in good agreement with those of $[KrF][MF_6]$ [133.7(1) (As), 139.2(2) (Sb), 138.(3)° (Bi)] and contrast with those of $[KrF][AsF_6]$ (124.6(3)°) in $[Kr_2F_3][AsF_6]\cdot[KrF][AsF_6]$ and $[XeF][Sb_2F_{11}]$ (149(2)°).[33] The differences likely arise from differences in the crystal packings and the deformabilities of the Ng- -F_b- -M angles (see Computational Results).

Synthesis and Characterization by Raman Spectroscopy of $[Kr_2F_3][PF_6]\cdot nKrF_2$. Neither $[KrF][PF_6]$ and $[Kr_2F_3][PF_6]$

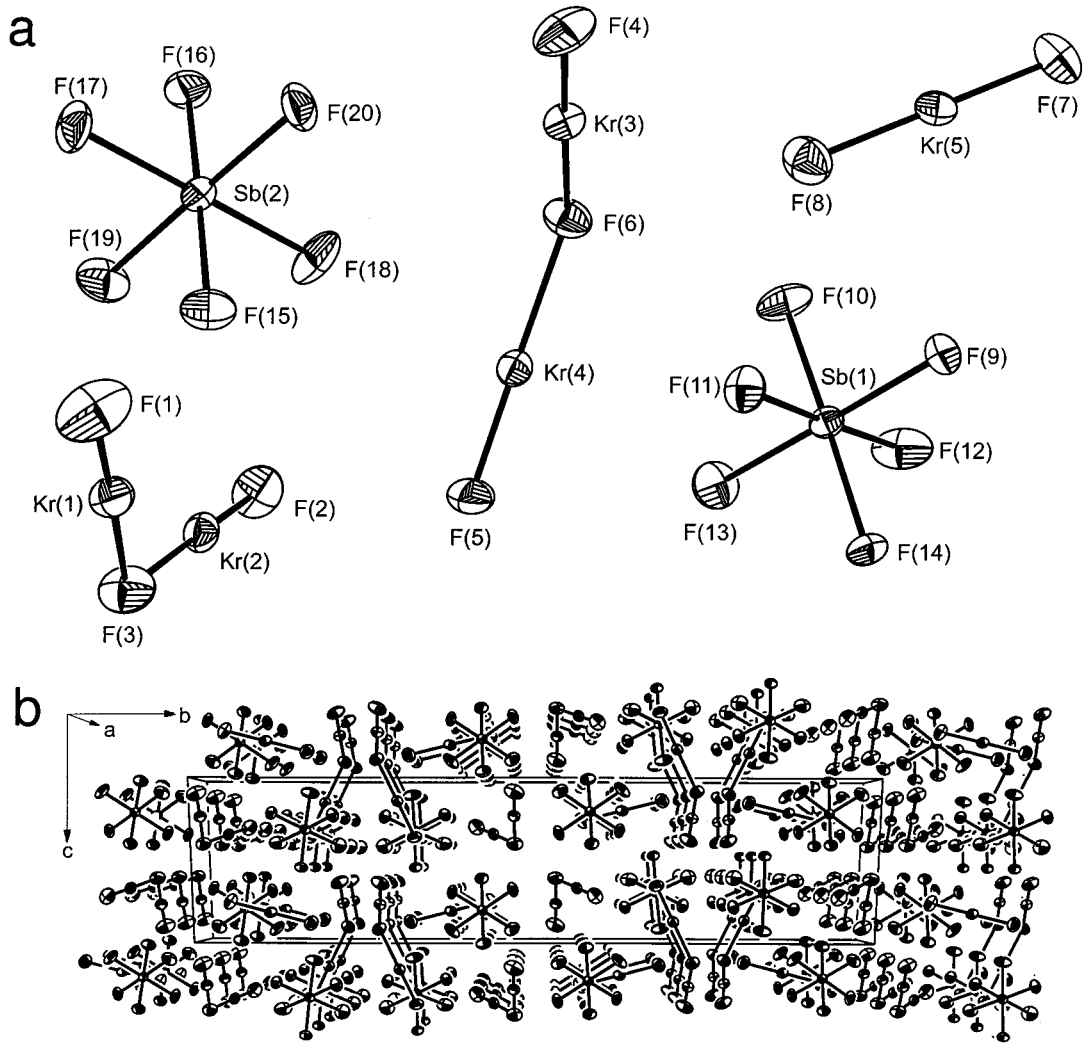

Figure 4. (a) Structure of $[Kr_2F_3]_2[SbF_6]_2 \cdot KrF_2$ and (b) view of the $[Kr_2F_3]_2[SbF_6]_2 \cdot KrF_2$ unit cell along the *a*-axis; thermal ellipsoids are shown at the 50% probablility level.

nor their xenon(II) analogues have been reported previously. Attempts, in the present work, to synthesize KrF^+ and $Kr_2F_3^+$ salts of the PF_6^- anion by reaction of KrF_2 with excess PF_5 in anhydrous HF solvent at −78 °C failed. Reaction of KrF_2 with liquid PF_5 at −78 °C, however, yielded $[Kr_2F_3][PF_6] \cdot nKrF_2$, where *n* is unspecified. The complete conversion to $[Kr_2F_3][PF_6] \cdot nKrF_2$ required nearly 2 months and was deemed complete upon the disappearance of the intense $\nu_1(\Sigma^+_g)$ vibrational mode of free KrF_2 at 465.5 cm^{-1} (α-phase) or 468.6 and 469.5 cm^{-1} (*β*-phase) in the Raman spectrum, during which time modes consistent with $Kr_2F_3^+$ and PF_6^- became more intense. Further addition of fresh aliquots of PF_5 to $[Kr_2F_3][PF_6] \cdot nKrF_2$ did not result in $[KrF][PF_6]$ or any further changes in the Raman spectrum over an additional 2 month period. The salt was isolated at −78 °C as a white solid under 1000 Torr of PF_5(g). The $[Kr_2F_3][PF_6] \cdot nKrF_2$ adduct rapidly dissociated to KrF_2 and PF_5 under reduced PF_5 pressures at −78 °C.

The Raman spectrum of $[Kr_2F_3][PF_6] \cdot nKrF_2$ (Figure 6) was acquired under 1000 Torr of PF_5 at −80 °C after 7 weeks of contact between KrF_2 and PF_5 at −78 °C and closely resembles the spectra of the $[Kr_2F_3][MF_6] \cdot nKrF_2$ (M = As, Sb) salts (Table 5). The assignments of the $[Kr_2F_3][PF_6] \cdot nKrF_2$ spectrum were consequently based on those of the AsF_6^- and SbF_6^- analogues and were verified with the aid of theoretical calculations (see Computational Results). The PF_6^- anion spectrum was identified by the A_{1g} (748 cm^{-1}), E_g (572 and 581 cm^{-1}), and T_{2g} (464, 469, and 475 cm^{-1}) modes, which are consistent with an octahedral anion for which site symmetry lowering apparently results in removal of the degeneracies of the E_g and T_{2g} modes.[51] The intense bands at 555 and 605 cm^{-1} are assigned under C_{2v} symmetry to the asymmetric and symmetric Kr−F_t stretches, $\nu_6(B_1)$ and $\nu_1(A_1)$, respectively, of the $Kr_2F_3^+$ cation. It is noteworthy that, like $[Kr_2F_3][AsF_6] \cdot nKrF_2$ and $[Kr_2F_3][SbF_6] \cdot nKrF_2$, the 605 cm^{-1} band is not factor-group split but is split in $[Kr_2F_3][AsF_6]$ and $[Kr_2F_3][SbF_6]$. The weak band at 358 cm^{-1} is assigned to $\nu_2(A_1)$, the symmetric Kr- -F_b- -Kr stretch, and the coupled in-plane and out-of-plane bends associated with the F_t-Kr- -F_b groups are assigned to the medium intensity bands $\nu_9(B_2)$ 191, $\nu_3(A_1)$ 185, and $\nu_5(A_2)$ 176 cm^{-1}. The aforementioned show negligible dependence on the counteranion, which is also true of the AsF_6^- and the SbF_6^- salts,[13,16] and is consistent with a $Kr_2F_3^+$ cation that interacts weakly with the PF_6^- anion. The Raman spectrum (Figure 6) also revealed a trace impurity in the sample, which exhibited weak vibrational frequencies at 1859 and 1863 cm^{-1}. The bands are assigned to the O_2^+ cation and are in good agreement with the O_2^+

(51) Heyns, A. M. *Spectrochim. Acta* **1977**, *33A*, 315.

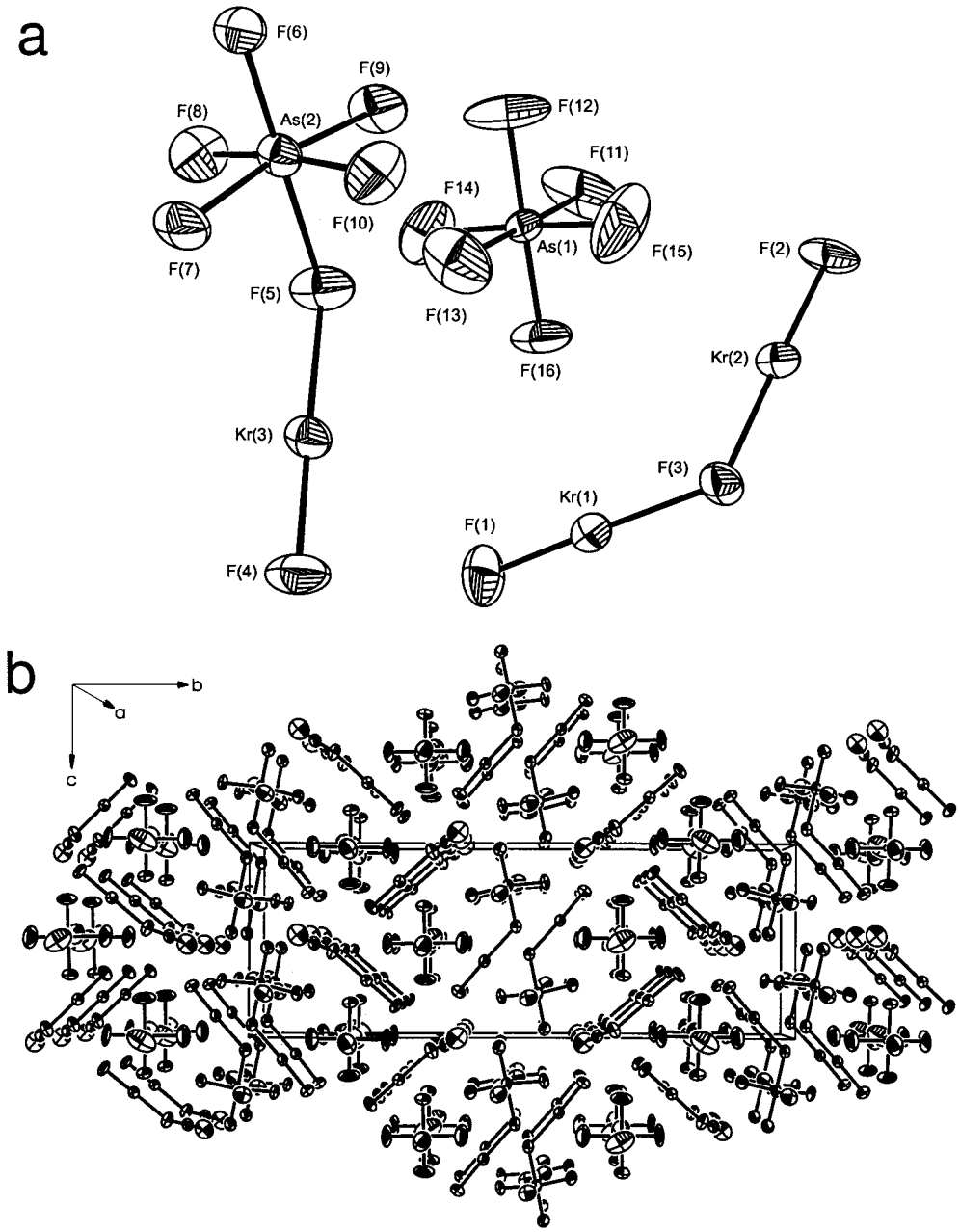

Figure 5. (a) Structure of $[Kr_2F_3][AsF_6]\cdot[KrF][AsF_6]$ and (b) view of the $[Kr_2F_3][AsF_6]\cdot[KrF][AsF_6]$ unit cell along the *a*-axis; thermal ellipsoids are shown at the 50% probability level.

frequencies observed for $[O_2][MF_6]$ (M = As, Sb, Bi, Ru, Rh, Pd, Pt, Au).[52] The $[O_2][PF_6]$ contaminant arises from the oxidation of trace amounts of H_2O and/or O_2 by the strongly oxidizing $Kr_2F_3^+$ cation.[16] The band splitting is likely attributable to a mixture of α- and β-$[O_2][PF_6]$ that apparently coexist near the phase-transition temperature as noted for $[O_2][AsF_6]$[53,54] and $[O_2][AuF_6]$.[55]

Computational Results

Dixon et al.[56] have previously used ab initio calculations at the Hartree−Fock (HF) level to obtain the energy-minimized geometries and electronic properties of $Xe_2F_3^+$ and the isoelectronic analogue, $XeIF_3$, defining for the first time the 5c−6e hypervalent bond. In these studies, the HF method predicted a linear structure for $Xe_2F_3^+$. This contrasts with the bent structure observed for $Xe_2F_3^+$ in its crystal structures in which the Xe- -F_b- -Xe bond angle ranges from 139.8(8) to 160.3(3)°.[37,38] In a more recent study, the local density-functional theory (LDFT) results for $Xe_2F_3^+$ are in better agreement with the experiment than the HF values, predicting a bent Xe- -F_b- -Xe angle (146.9°).[38] In the present study, we have used both HF and LDFT electronic structure calculations to characterize KrF_2, KrF^+, $Kr_2F_3^+$, and the fluorine-bridged ion pairs $[KrF][MF_6]$ (M = P, As, Sb, Bi).

Geometries. (a) KrF_2. The optimized HF and LDFT geometries of KrF_2 (Table 2) are linear with Kr−F bond lengths of 1.822 and 1.910 Å, respectively, with the LDFT method

(52) Griffiths, J. E.; Sunder, W. A.; Falconer, W. E. *Spectrochim. Acta* **1975**, *31A*, 1207.
(53) Naulin, C.; Bougon, R. J. *J. Chem. Phys.* **1976**, *64*, 4155.
(54) Griffiths, J. E.; Sunder, W. A. *J. Chem. Phys.* **1982**, *77*, 1087.
(55) Lehmann, J. F.; Schrobilgen, G. J. Unpublished results.
(56) Dixon, D. A.; Arduengo, A. J., III.; Farnahm, W. B. *Inorg. Chem.* **1989**, *28*, 4589.

Table 5. Experimental Raman and Calculated Vibrational Frequencies, Assignments, and Mode Descriptions for $Kr_2F_3^+$

$[Kr_2F_3][AsF_6]^{a,b}$	$[Kr_2F_3][SbF_6]^{a,b}$	$[Kr_2F_3][PF_6]\cdot nKrF_2^{b,c}$	$[Kr_2F_3][AsF_6]\cdot nKrF_2^{a,b}$	$[Kr_2F_3][SbF_6]\cdot nKrF_2^{a,b}$	LDFT[d]	assignments for $Kr_2F_3^+$ in C_{2v} point group[e]
610(43), 600(80), 594(100)	603(100), 594(89)	605(100)	602(100)	599(100)	628(12)	$\nu_1(A_1)$ $\nu(KrF_t + KrF_t)$
570(4), 567(31)	555(34)	555(52)	575(23), 553(50)	557(50)	608(273)	$\nu_6(B_1)$ $\nu(KrF_t - KrF_t)$
437(5)	456(4)	462(11)	462	466(60)	441(212)	$\nu_7(B_1)$ $\nu_{as}(KrF_b)$
347(sh), 336(17)	330(18)	358(19)	355(19)	340(14)	313(11)	$\nu_2(A_1)$ $\nu_s(KrF_b)$
183(15)	186(16)	191(11)	190(10)	200(2)	196(14)	$\nu_9(B_2)$ $\delta(F_t{-}Kr{-}\cdot\cdot{-}F_b)$ oop antisym comb
174(13)	180(sh)	185(7)	184(sh)	188(10)	168(1)	$\nu_3(A_1)$ $\delta_s(F_t{-}Kr{-}F_b)$ ip sym comb
158(2)	176(sh)	176(5)	177(sh)	122(46)	159(0)	$\nu_5(A_2)$ $\delta(F_t{-}Kr{-}\cdot\cdot{-}F_b)$ oop sym comb
					155(0)	$\nu_8(B_1)$ $\delta(F_t{-}Kr{-}\cdot\cdot{-}F_b)$ ip antisym comb
					41(0)	$\nu_4(A_1)$ $\delta(Kr{-}\cdot\cdot{-}F_b{-}\cdot\cdot{-}Kr)$ bend

[a] From ref 16; anion modes are also given in this reference. The abbreviation, sh, denotes a shoulder. [b] Values in parentheses denote relative Raman intensities. [c] Frequencies observed for PF_6^-: 748(7) $\nu_1(A_{1g})$; 581(7) and 572(13), $\nu_2(A_{1g})$; 475(12), 469(35), and 464(11), $\nu_5(T_{2g})$. Spectrum recorded on a powder in a $^1/_4$-in. FEP sample tube at −80 °C using 514.5 nm excitation. Values in parentheses denote relative Raman intensities. Additional weak bands were observed at 1859(0.20) and 1863(0.15) cm^{-1} that are assigned to O_2^+. [d] Infrared intensities, in km mol^{-1}, are given in parentheses. [e] The abbreviations oop and ip denote out of plane and in plane, respectively.

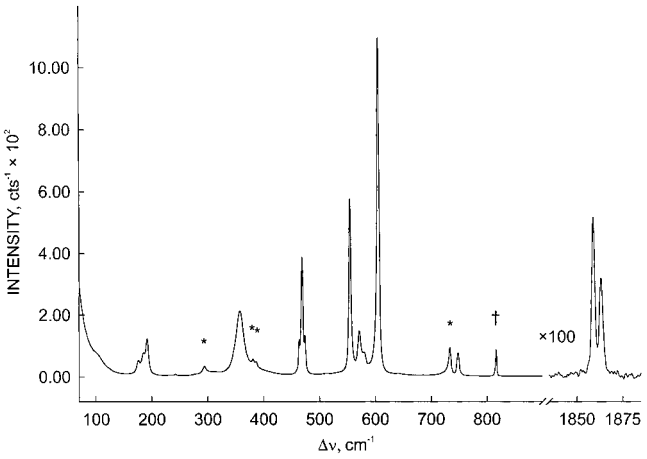

Figure 6. Raman spectrum of powdered $[Kr_2F_3][PF_6]\cdot nKrF_2$ recorded at −80 °C using 514.5 nm excitation. Peaks arising from the FEP sample tube are denoted by asterisks (*), while that resulting from excess PF_5 is denoted by a dagger (†).

predicting longer distances and providing better agreement with the experimental values.

(b) KrF^+ and $[KrF][MF_6]$. Two conformers having C_s point symmetry are found for the energy-minimized gas-phase structures of the $[KrF][MF_6]$ ion pairs (Table 3). The theoretical structures for $[KrF][PF_6]$ and $[KrF][AsF_6]$ have the F_t-Kr- -F_b moiety in an MF_3 plane (Structure VII), whereas for $[KrF][SbF_6]$

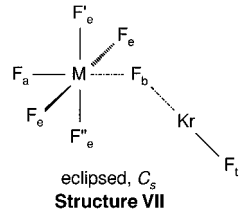

Structure VII

and $[KrF][BiF_6]$, the F_t-Kr- -F_b moiety is rotated by 45° so that it is staggered and lying in the mirror plane that bisects the angle subtended by two equatorial fluorine atoms of the axially distorted MF_6^- anion (Structure VIII). The staggered structure is more stable than the eclipsed one by 0.7 kcal mol^{-1} for $[KrF][SbF_6]$ and by 0.8 kcal mol^{-1} for $[KrF][BiF_6]$. In contrast, this angle ranges from 19.7 to 28.1° in the experimental structures,

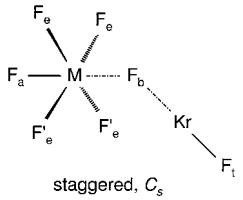

Structure VIII

and consequently, their deviations from the calculated values are attributed to crystal packing.

The bond length of free KrF^+ was calculated to be 1.780 Å (LDFT) and 1.717 Å (HF). The LDFT values for the Kr−F_t bond length do not show as pronounced variations for the structures of the ion pairs (1.857−1.877 Å) as the HF values do, which predict a longer bond in $[KrF][PF_6]$ (1.789 Å) than in $[KrF][AsF_6]$ (1.746 Å), $[KrF][SbF_6]$ (1.739 Å), and $[KrF][BiF_6]$ (1.739 Å). Surprisingly, the experimental Kr−F_t bond lengths are most accurately approximated by the bond length of free KrF^+, which is overestimated by the same magnitude (∼0.01 Å) as those calculated for KrF_2 and the Kr−F_t bond lengths of $Kr_2F_3^+$ using LDFT. It should be noted that the LDFT Kr−F_t bond lengths in the ion pairs are longer than the free KrF^+ value by ∼0.09 Å and are also predicted to be longer than the Kr−F_t bond lengths of $Kr_2F_3^+$.

LDFT predicts that the KrF_2 interaction with the weak fluoride ion acceptor, PF_5, is better described as a $KrF_2\cdot PF_5$ adduct than the ionic complex $[KrF][PF_6]$. The KrF_2 moiety in this species is asymmetric with a Kr- -F_b bond length of 1.972 Å and a Kr−F_t bond length of 1.877 Å. The Kr- -F_b bond is 0.06 Å longer, and the Kr−F_t bond is 0.03 Å shorter than the calculated bond distance in KrF_2, while Kr−F_t in $KrF_2\cdot PF_5$ is 0.10 Å longer than the bond in free KrF^+. The P- -F_b bond distance of 2.176 Å is lengthened by 36% when compared with the average bond length of the equatorial P−F bonds (1.595(9) Å). The M- -F_b bridge distances for the heavier pnicogens in $[KrF][MF_6]$ are 2.096 (As), 2.185 (Sb), and 2.266 (Bi) Å, and the Kr- -F_b bridge bond distances are 1.998 (As), 2.017 (Sb), and 2.012 (Bi) Å with shorter terminal Kr−F_t bond distances of 1.867 (As), 1.857 (Sb), and 1.859 (Bi) Å. The experimental structures likewise fail to show a consistent trend among Kr- -F_b distances [2.131(2) (As), 2.140(3) (Sb), and 2.089(6) (Bi) Å] and Kr−F_t [1.765(2) (As), 1.765(3) (Sb), and 1.774(6) (Bi) Å] bond lengths. The

calculated M- -F_b distances are 21 (As), 14 (Sb), and 15% (Bi) longer than the average of the equatorial M−F bond lengths: 1.737(10) (As), 1.916(10) (Sb), and 1.967(12) (Bi) Å. The comparison is particularly noteworthy for P and As, which have similar averaged equatorial M−F bond lengths. The degree of fluoride ion transfer from KrF_2 to the strong fluoride ion acceptor, AsF_5, is considerably greater than for PF_5. The M- -F_b interactions and degrees of F^- transfer are greatest for SbF_5 and BiF_5, where the M- -F_b bond lengths are only ∼15% longer than the average equatorial M−F bond length. This trend is consistent with the fluoride ion affinities of the parent MF_5 molecules, which have been calculated to be PF_5 (94.9 kcal mol^{-1}) < AsF_5 (105.9 kcal mol^{-1}) < SbF_5 (120.3 kcal mol^{-1}).[57] Comparison of the calculated structures with the experimental structures shows that the degree of fluoride ion transfer from MF_6^- to KrF^+ in the crystal is substantially less than is predicted for the gas-phase species. The experimental M- -F_b bond lengths were determined to be 1.845(2), 1.963(3), and 2.105(6) Å for As, Sb, and Bi, respectively, and are only 8, 6, and 8% longer than the average of their respective experimental equatorial M−F bonds.

The F_t-Kr- -F_b angles in the $[KrF][MF_6]$ ion pairs are predicted to be slightly distorted [178.3 (P), 177.7 (As), 177.4 (Sb), and 177.2 (Bi)°] from linearity, and similar angle distortions are observed in the experimental structures [176.8(1) (As), 177.9(2) (Sb), and 177.0(4) (Bi)°]. The Kr- -F_b- -M angles [120.0 (As), 114.1 (Sb), and 113.8 (Bi)°] are predicted to be more closed than in the experimental structures [133.7(1) (As), 139.2-(2) (Sb), and 138.3(3) (Bi)°], where crystal packing apparently requires more open angles. The consistency of the experimental angles is likely a consequence of their isomorphous packing arrangements. The explanation is supported by the observation that the Kr- -F_b- -As angle (124.6(3)°) in the $[KrF][AsF_6]$ unit of the nonisomorphous double salt, $[Kr_2F_3][AsF_6]\cdot[KrF][AsF_6]$, is more closed than in β-$[KrF][AsF_6]$ and is in better agreement with the theoretical value. These angles are expected to be highly deformable and susceptible to crystal packing effects, on the basis of the low calculated gas-phase frequencies of their bending modes [73 (As), 80 (Sb), and 74 (Bi) cm^{-1}].

(c) $Kr_2F_3^+$. As in a previous study of $Xe_2F_3^+$,[38] the LDFT method predicts a bent structure for $Kr_2F_3^+$ in agreement with the experiment, whereas the HF method predicts a linear structure (Table 4). As expected from the results for KrF_2, the LDFT method predicts the Kr−F_t bond lengths to be too long by ∼0.03 Å. Similarly, the Kr- -F_b bond length is predicted to be too long by 0.02−0.05 Å, depending on the structure. The linear structure predicted by the HF method has a Kr−F_t bond distance that is too short (1.730 Å) and a Kr- -F_b bond distance that is too long (2.082 Å).

As previously noted for KrF_2, the predicted bond lengths bracket the Kr−F_t bond length with a slight overestimation (∼0.02 Å) by LDFT and a larger underestimation (∼0.07 Å) by HF theory. Both LDFT and HF theory overestimate the Kr- -F_b bond length, arriving at similar values of 2.081 and 2.082 Å, respectively. In a previously published study, LDFT was shown to predict F_t-Xe- -F_b (178.3°) and Xe- -F_b- -Xe (146.9°) bond angles in $Xe_2F_3^+$ with reasonable accuracy.[38] Likewise, LDFT predicts F_t-Kr- -F_b and Kr- -F_b- -Kr bond angles of 177.4 and 135.2°, respectively, which lie within their respective experimental bond angle ranges of 175.1(2)−178.6(3) and 126.0(2)−142.4(3)°. Moreover, in both the experimental and calculated structures, the F_t atoms are bent away from each other and lie in the Kr- -F_b- -Kr plane to give a W-shaped structure. The persistence of these bond angles in the gas phase indicates that they are intrinsic properties of the cation, although packing effects and long contacts in the solid state are undoubtedly responsible for the bond angle variations observed among the different salts.

The nonlinear F_t-Kr- -F_b bond angles result from a number of factors. The overall molecule is bent with a Kr- -F_b- -Kr bond angle of 135° and an asymmetric environment about the krypton with two inequivalent fluorine atoms. Thus, there is no symmetry constraint to keep the F_t-Kr- -F_b bond angle linear. The bond angle deviates by less than 3° from 180°, leading to an increase in the distance between F_t atoms. We note that the molecule is quite floppy with F_t-Kr- -F_b bending frequencies less than 170 cm^{-1}. The deviation from linearity likely arises because the bonding about krypton is no longer as symmetric as it is in KrF_2. Thus, the 3c−4e hypervalent bond at krypton can build in other orbital character and deviate from linearity. The bonding in $Kr_2F_3^+$ has a strong component of two KrF^+ cations bonding to the central F^- ion. With no orbital symmetry constraint, the bond angles at the Kr can adjust to maximize the interactions with F_b and minimize any repulsive interactions.

Vibrational Frequencies. The vibrational frequencies of KrF_2, $Kr_2F_3^+$, KrF^+, and the $[KrF][MF_6]$ ion pairs have been determined using HF and LDFT calculations. Comparison of the two methods reveals that the vibrational frequencies predicted by the LDFT method are more accurate than those predicted by the HF method. HF theory was found to overestimate the vibrational frequencies by 12−143 cm^{-1}, in accord with the shorter bond lengths predicted at this level of theory. Moreover, the geometry of $Kr_2F_3^+$ calculated at the HF level is linear and not bent as arrived at by LDFT and observed experimentally. Despite the significant difference in the LDFT and HF bond lengths and bond angles, the frequency orderings are essentially identical using the two levels of theory. Only the vibrational frequencies predicted by LDFT theory are compared in the ensuing discussion.

(a) KrF_2. LDFT predicts the vibrational modes of KrF_2 to occur at $\nu_1(\Sigma^+_u)$ 623, $\nu_2(\Sigma^+_g)$ 504, and $\nu_3(\Pi_u)$ 228 cm^{-1}, which are in reasonable agreement with those found experimentally (596/580, 449, and 233 cm^{-1}).[58] The Kr−F stretch of free KrF^+ is predicted to be at 686 cm^{-1} and is significantly higher than the symmetric stretching frequency of KrF_2. The difference is consistent with the 2c−2e and 3c−2e descriptions of KrF^+ and KrF_2, which lead to formal bond orders of 1 and $^1/_2$, respectively. The experimental Kr−F stretching frequencies for the KrF^+ salts we have considered in the present work range from 607 to 619 cm^{-1}. The high value of the stretching frequency of the free KrF^+ cation, relative to that of coordinated KrF^+ in its salts, is consistent with a significant fluorine bridge interaction between the cation and anion, which leads to longer and more ionic Kr−F_t bonds in the ion pairs.

(b) $Kr_2F_3^+$. The calculated LDFT vibrational frequencies of the Kr−F_t stretches of $Kr_2F_3^+$ (Table 5) are also significantly lower than the Kr−F stretching frequency of free KrF^+ and are consistent with a significant bonding interaction between the KrF^+ cations and the bridging F^-. The calculated values are in excellent agreement with the experimental frequencies, with calculated values for the Kr−F_t stretching modes at $\nu_6(B_1)$, 608 and $\nu_1(A_1)$, 628 cm^{-1} and for the Kr- -F_b stretching modes at $\nu_2(A_1)$, 313 and $\nu_7(B_1)$, 441 cm^{-1}. The previous experimental assignments for $\nu_1(A_1)$ and $\nu_6(B_1)$ are, however, reversed with

(57) Christe, K. O.; Dixon, D. A.; McLemore, D. K.; Wilson, W. W.; Sheehy, J. A.; Boatz, J. A. *J. Fluorine Chem.* **2000**, *101*, 151.

(58) Claassen, H. H.; Goodman, G. L.; Malm, J. G.; Schreiner, F. *J. Chem. Phys.* **1965**, *42*, 1229.

respect to the theory-based assignments and have been reassigned accordingly in Table 5. The F_t-Kr- -F_b in-plane and out-of-plane bending modes are in good agreement with the experimental values. The in-plane bending frequency corresponding to the deformation of the Kr- -F_b- -Kr angle is very low, 41 cm^{-1}. Thus, the various interactions within the crystal could easily distort this angle because the potential energy surface for bending is so flat. Similar deformabilities have been noted for the Xe- -F_b- -Xe angles in several $Xe_2F_3^+$ salts[37,38] when compared with their theoretical gas-phase values.

(c) [KrF][MF_6]. A difficulty arises when assigning the vibrational spectra of the ion pairs. In the idealized case of complete fluoride ion transfer, an octahedral MF_6^- anion (O_h point symmetry) results, and only the Raman-active $\nu_1(A_{1g})$, $\nu_2(E_g)$, and $\nu_5(T_{2g})$ modes and the infrared-active $\nu_3(T_{1u})$ and $\nu_4(T_{1u})$ modes are observed in addition to ν(Kr−F) of the cation. Because complete fluoride ion transfer is never achieved in the solid state, except when the cation is coordinately saturated as in $Kr_2F_3^+$ salts, the anion symmetry is primarily distorted by the elongation of the bond involved in fluorine bridging to the cation, namely, M- -F_b. The secondary fluorine bridge interaction results in lowering of the anion symmetry and the observation of additional bands in the vibrational spectra. The symmetry lowering is oftentimes approximated as C_{4v} symmetry,[14−17,59,60] and the vibrational spectra are assigned under this or a lower point symmetry such as C_s symmetry[59,60] to allow for the bent nature of the Ng- -F_b- -M moiety (where Ng is the central Kr or Xe atom of the cation). Along with the tentative assignments and approximate mode descriptions for the fluorine-bridged anion, attempts have been previously made to assign the vibrational modes associated with the Ng- -F_b- -M bridge.[14−17,59,60] We now report the mode descriptions and the frequency assignments derived from LDFT and HF calculations for the fluorine-bridged F_t-Kr- -F_b- -MF_5 ion pairs. The assignments and their descriptions (Tables 6−9) are for eclipsed (M = P, As; Structure VII) and staggered (M = Sb, Bi; Structure VIII) gas-phase conformations having C_s point symmetries. Although the conformations of the ion pairs are skewed to give C_1 point symmetry in their crystal structures and not all of the predicted frequencies have been observed, the approach provides more complete assignments and more precise descriptions of the vibrational modes in these strongly coupled systems than have been available previously.[16] Assignments and descriptions of the vibrational modes of the MF_5 moiety are provided without further comment.

The calculated Kr−F_t stretches of the gas-phase [KrF][MF_6] ion pairs occur at 611 (As), 616 (Sb), and 616 (Bi) cm^{-1} and are in excellent agreement with the experimental values, which are also insensitive to the degree of F^- ion transfer. The lower frequency Kr- -F_b stretches, which are predicted at 454 (As), 357 (Sb), and 436 (Bi) cm^{-1}, are in good agreement with the experiment. Direct comparison of the Kr- -F_b stretching mode is not possible because of significant coupling to Kr−F_t (As) and to MF_5 modes (Sb). Only in [KrF][BiF_6] is the Kr- -F_b stretch not significantly coupled. The Kr−F_t and Kr- -F_b stretches of the PF_6^- compound, for which there are no experimental values, are both strongly coupled to anion modes and cannot be compared with other members of the series.

Mayer Bond Orders and Valencies and Mulliken Charges. One way to gain insight into the types of interactions involved is to use Mayer valency and bond order indices.[61−64] The Mayer bond orders, Mayer valencies, and atomic charges for KrF_2, KrF^+, $Kr_2F_3^+$, and the [KrF][MF_6] ion pairs have been estimated using the electronic structures derived from LDFT calculations (Table 10). The Kr−F_t bond orders were found to have little

Table 6. Calculated Vibrational Frequencies, Assignments, and Mode Descriptions for [KrF][PF_6]

frequencies (cm^{-1})		
LDFT[a]	HF[a]	assignments (C_s)[b]
951(358)	1085(437)	A″ $\nu_{as}(PF_{2e})$
937(305)	1071(413)	A′ $\nu(PF'_e)$
917(375)	1052(382)	A′ $\nu(PF_a)$
735(8)	859(8)	A′ $\nu_s(PF_5)$
616(71)	694(5)	A′ $\nu_s(PF_{2e}) - \nu_s(PF'_e) - \nu_s(PF''_e) + \nu(KrF_t)$
613(100)	676(250)	A′ $\nu_s(PF_{2e}) - \nu_s(PF'_e) - \nu_s(PF''_e) - \nu(KrF_t)$
515(32)	598(109)	A′ $\delta(PF_{2e}) + \delta(F_aPF'_e - F_aPF''_e)$
511(38)	592(57)	A″ $\delta(F'_ePF''_e) + \delta(F_aPF_e - F_aPF_e)$
499(1)	587(5)	A″ $\delta(F''_ePF_e) + \delta(F'_ePF_e)$
497(21)	580(27)	A′ $\delta(PF_{2e}) + \delta(PF'_eF''_e)$ oop + $\nu_s(KrF_2)$
436(113)	505(283)	A′ $\nu(KrF''_e) + \nu(KrF_b) + \delta(PF_{2e}F'_eF''_e)$ oop
358(0)	402(6)	A″ $\delta(F_ePF_a) - \delta(F_aPF_e) + \delta(F_ePF_b) - \delta(F_ePF_b)$
341(20)	387(0)	A′ $\delta(F_aPF''_e)$ ip − $\delta(F_aPF'_e)$ ip
278(117)	312(83)	A′ $\nu(KrF_b) + \delta(F_tKrF_b)$ ip
247(6)	304(20)	A″ $\delta(F_tKrF_b)$ oop
190(0)	149(0)	A′ $\delta(F'_ePF''_e)$ ip − $\delta(F_ePF_e)$ along F_a−P−F_b
164(3)	145(5)	A″ $\delta(F_tKrF''_e)$ oop + torsion about PF''_e
155(6)	112(5)	A′ $\delta(F'_ePF''_e) - \delta(F_tKrF''_e)$ ip
127(17)	75(10)	A′ $\nu(P-F_b)$
81(0)	52(3)	A′ $\delta(PF_bKr) + \nu(KrF''_e)$
23(0)	10i(0)	A″ torsion of KrF_2 group about the P−F_b bond + rock of PF_5 group toward KrF_2

[a] Infrared intensities, in km mol^{-1}, are given in parentheses. [b] The atom labeling scheme is given in Structure VII; oop and ip denote out of plane and in plane, respectively.

Table 7. Experimental Raman Frequencies and Calculated Vibrational Frequencies, Assignments, and Mode Descriptions for β-[KrF][AsF_6]

frequencies (cm^{-1})			
LDFT[a]	HF[a]	exp[b]	assignments (C_s)[c]
745(152)	824(199)		A″ $\nu_{as}(AsF_{2e})$
737(129)	819(192)		A′ $\nu(AsF'_e) - \nu(AsF''_e) - \nu(AsF_a)$
730(123)	813(114)	716(16)	A′ $\nu(AsF'_e) - \nu(AsF''_e) + \nu(AsF_a)$
652(16)	745(57)	676(13)	A′ $\nu_s(AsF_5)$ + small $\nu(AsF_a)$
611(179)	735(113)	615(100), 619(72)	A′ $\nu(KrF_t) - \nu(KrF_b)$
601(0)	650(4)	595(5)	A′ $\nu(AsF''_e + AsF'_e) - \nu(AsF_{2e})$
454(23)	498(128)	464(3)	A′ $\nu(KrF_b) - \nu(AsF_b)$ + some $\nu(KrF_t)$
		411(10), 419 sh	unassigned AsF_6^- bands[d]
361(16)	447(63)	384(4)	A″ $\delta(F_eAsF''_e) - \delta(F_eAsF''_e)$
356(14)	434(52)	366(9)	A′ $\delta(F_bAsF''_e) + \delta(F_eAsF_e)$ along F'_e−As−F''_e
340(25)	425(35)	338(16)	A″ $\delta(F'_eAsF_e) - \delta(F'_eAsF_e)$
335(24)	406(13)		A′ $\delta(F_eAsF_e) + \delta(F''_eAsF_b)$ along F'_e−As−F''_e
289(199)	365(0)	273(1)	A′ $\nu(AsF_b) + \delta(AsF_{2e}F'_eF''_e)$ oop
280(0)	315(157)		A″ $\delta(F_bAsF_e) + \delta(F_aAsF_e)$
249(7)	299(376)		A′ $\delta(F''_eAsF_a) + \delta(F'_eAsF_b) + \nu(F_bKr)$
225(5)	282(5)		A″ $\delta(F_tKrF_b)$ oop + $\delta(F_bKrF_a)$
171(1)	222(1)	173(10)	A′ $\delta(F_eAsF_e) - \delta(F''_eAsF_e)$
155(6)	197(3)	162(11)	A′ $\delta(F_tKrF''_e)$ ip + $\nu(AsF_b)$
149(1)	185(41)		A″ $\delta(F_tKrF_b)$ oop + (AsF_5) rock oop
137(1)	168(9)		A′ $\delta(F''_eAsF_b) - \delta(F'_eAsF_b)$
73(0)	70(0)		A′ $\delta(KrF_bAs)$
4(0)	21i(0)		A″ torsion of KrF_2 group about the As−F_b bond + rock of AsF_5 group toward KrF_2

[a] Infrared intensities, in km mol^{-1}, are given in parentheses. [b] Experimental values are taken from ref 16. The abbreviation, sh, denotes a shoulder. Values in parentheses denote relative Raman intensities. [c] The atom labeling scheme is given in Structure VII; oop and ip denote out of plane and in plane, respectively. [d] Similar bands have been observed in other AsF_6^- salts but are not assigned.

(59) Sladky, F. O.; Bulliner, P. A.; Bartlett, N. *J. Chem. Soc. A* **1969**, 2179.
(60) Gillespie, R. J.; Landa, B.; Schrobilgen, G. J. *Inorg. Chem.* **1976**, *15*, 1256.

Table 8. Experimental Raman Frequencies and Calculated Vibrational Frequencies, Assignments, and Mode Descriptions for [KrF][SbF_6]

frequencies (cm^{-1})			
LDFT[a]	HF[a]	exp[b]	assignments[c] (C_s)
668(94)	748(72)	682(3)	A′ $\nu_{as}(SbF_e - SbF'_e) + \nu_{as}(SbF_a) + \nu_{as}(SbF'_e - SbF_e)$
666(94)	727(134)	664(45)	A″ $\nu(SbF'_e - SbF_e) + \nu(SbF_e - SbF'_e)$
661(72)	725(139)	642(10)	A′ $\nu(SbF_a) - \nu(SbF'_e + SbF'_e)$
616(170)	719(113)	615(100), 619(74)	A′ $\nu(KrF_t) + \nu(SbF_{2e} + SbF'_{2e})$
600(5)	677(38)		A′ $\nu(SbF_{2e} + SbF'_{2e})$ + small $\nu(SbF_a)$ − small $\nu(KrF_t)$
581(4)	613(4)	586(5)	A′ $\nu(SbF_e + SbF'_e) - \nu(SbF_e + SbF'_e)$
439(64)	439(239)	462(8), 480(4)	A′ $\nu(KrF_b) + \nu(KrF_t)$
357(43)	413(31)	338(4)	A′ $\nu(SbF_b)$
253(47)	331(82)	288(9)	A′ $\delta(F'_eSbF'_e)$
246(44)	327(12)	266(6)	A″ $\delta(F_bSbF_a)$ oop $\delta(F_tKrF_b)$
236(60)	311(78)	255(6)	A′ $\delta(F_eSbF_e)$
231(41)	300(19)		A′ $\delta(F_aSbF_b)$ ip + $\delta(F_eSbF_e) - \delta(F'_eSbF'_e)$
226(5)	294(268)	214(2)	A″ $\delta(F_tKrF_b)$ oop − $\delta(F_aSbF_b)$ oop
179(4)	236(35)	169(5)	A″ $\delta(F_tKrF_b) - \delta(F_bSbF_a)$
176(2)	227(2)	162(7)	A″ $\delta(F_aSbF_e) - \delta(F_eSbF'_e) + \delta(F_tKrF_b)$ oop
165(1)	194(2)	145(3)	A′ $\delta(F_tKrF_b)$ ip
139(0)	173(1)		A″ $\delta(F_aSbF_b)$ oop + $\delta(F_eSbF'_e)$ + $\delta(F_eSbF'_e)$
109(2)	152(0)		A′ $\delta(F_bSbF_a)$ ip − $\delta(SbF_bKr)$
91(0)	141(11)		A″ $\delta(F'_eSbF_e)$ oop − $\delta(F'_eSbF_e)$
80(0)	53(1)		A′ $\delta(SbF_bKr) + \delta(F_bSbF_a)$
54(0)	22(0)		A″ KrF_t torsion about SbF_b + (SbF_5) rock

[a] Infrared intensities, in km mol^{-1}, are given in parentheses. [b] Experimental values are taken from ref 16. Values in parentheses denote relative Raman intensities. [c] The atom labeling scheme is given in Structure VIII; oop and ip denote out of plane and in plane, respectively.

Table 9. Experimental Raman Frequencies and Calculated Vibrational Frequencies, Assignments, and Mode Descriptions for [KrF][BiF_6]

frequencies (cm^{-1})			
LDFT[a]	HF[a]	exp[b]	assignments (C_s)[c]
616(149)	737(106)	604(11), 610(100)	A′ $\nu(KrF_t)$ − small $\nu(KrF_b)$
578(68)	691(83)	592(35), 600(11)	A′ $\nu(BiF_a)$
567(60)	690(119)	580(40)	A″ $\nu_{as}(BiF_{2e}) - \nu(BiF'_e)$
566(64)	689(93)		A″ $\nu_{as}(BiF_{2e}) - \nu(BiF'_e)$
537(6)	668(48)	547(3)	A′ $\nu_s(BiF_{2e} + BiF'_{2e})$
527(8)	614(8)	541(9)	A″ $\nu_{as}(BiF_{2e}) + \nu_{as}(BiF'_{2e})$
436(75)	446(368)		A′ $\nu(KrF_b)$
342(43)	374(31)	316(6)	A′ $\nu(BiF_b)$
234(22)	293(44)	244(5)	A″ $\delta(F_bKrF_t)$ oop − $\delta(F_bKrF_a)$
230(30)	258(0)	233(3), 225(1)	A′ $\delta(BiF'_{2e})$
213(65)	237(203)	209(5)	A′ $\delta(BiF_{2e})$
205(33)	236(67)	203(3)	A″ $\delta(F'_eBiF_a) - \delta(F'_eBiF_e) - \delta(F'_eBiF_e)$
201(35)	234(52)	193(4), 184(5)	A′ $\delta(F_eBiF'_e) + \delta(F_aBiF_b)$ ip
166(1)	199(1)		A″ $\delta(F_eBiF_a) + \delta(F_tKrF_b)$ oop
163(8)	193(6)	173(7)	A″ $\delta(F_eBiF_a) - \delta(F_eBiF_e)$
159(1)	184(15)		A′ $\delta(F_tKrF_b)$ ip + $\nu(F_bBi)$ + small $\delta(F_bBiF_a)$
127(0)	134(0)		A″ $\delta(F_bBiF_a)$ oop
100(1)	127(2)	117(4)	A′ $\delta(F_bBiF_a)$ ip + $\delta(KrF_bBi)$
84(0)	107(3)	87(7)	A″ $\delta(BiF_bKr)$ oop
74(0)	51(1)	81(10)	A′ $\delta(BiF_bKr)$ ip
43(0)	6i(0)		A″ KrF_t torsion about Bi−F_b + (BiF_5) rock

[a] Infrared intensities, in km mol^{-1}, are given in parentheses. [b] Experimental values are taken from ref 17. Values in parentheses denote relative Raman intensities. [c] The atom labeling scheme is given in Structure VIII; oop and ip denote out of plane and in plane, respectively.

dependence on the hexafluoropnicogen counteranion despite the strong fluorine bridge between the two ions and are in agreement with the constancy of the Kr−F_t bond lengths observed among the crystal structures of [KrF][MF_6] (M = As, Sb, Bi) (Table 3) and their calculated values (Table 3).

The atomic charges of KrF_2 were calculated to be 0.72 on krypton and −0.36 on each of the fluorine centers. For KrF^+, the full positive charge resides on krypton with zero charge on the fluorine atom. The Mayer bond order for uncoordinated KrF^+ is 1.09, and the valence at Kr is 1.09 as compared with the Kr−F bond order of KrF_2, which is reduced to 0.67 with a Kr valence of 1.35. There is considerable residual bond order between the terminal fluorine atoms in KrF_2. This arises because of the 3c−4e bond that can be used to describe the bonding in KrF_2. The 3c−4e bond leads to build up of density on the terminal atoms, and these atoms are linked through the 3c−4e bond, which is manifested in the residual bond order of 0.22.

The bond orders are similar for both $Ng_2F_3^+$ cations; however, the charges and valencies ($Xe_2F_3^+$ values are taken from ref 38 and are given in square brackets) show some noteworthy variations. The Kr- -F_b bridge bond order of $Kr_2F_3^+$ is 0.38 [0.40] while the Kr−F_t bond order of 0.86 [0.92] is intermediate with respect to that of free KrF^+ and KrF_2. The valence at the krypton atoms in $Kr_2F_3^+$ is 1.28 [1.37] and is slightly reduced with respect to that of KrF_2. The valencies for F_t, 1.04 [1.03], and F_b, 1.03 [0.94], are also similar, but the fluorine charges F_t, −0.37 [−0.24], and F_b, −0.16 [-0.46] and Ng atom charges, 0.85 [0.96], indicate that, relative to $Xe_2F_3^+$, a significant amount of charge has shifted from the bridge fluorine onto the Kr−F_t group. The charge on F_t (−0.37) of $Kr_2F_3^+$ is very similar to those on the fluorines of KrF_2 (−0.36) and that of F_b (−0.16) is intermediate with respect to that of KrF^+ (0.00) and KrF_2. The charge distributions indicate that the bridge fluorine of $Kr_2F_3^+$ is, next to the fluorine of KrF^+, the most electrophilic fluorine in the series under discussion. There is again a significant bond order for F_t- -F_b (0.14) in the $Kr_2F_3^+$ cation, which is reduced with respect to that of KrF_2 (0.22) but significantly greater than that in $Xe_2F_3^+$ (0.08).[65] The 5c−6e bond that can be used to qualitatively describe the bonding in $Kr_2F_3^+$ shows that there is an interaction between the F_b and F_t atoms resulting in a bond order of 0.14 for each $F_t \cdots F_b$ interaction. The lengthening of the Kr−F_b bond and the decrease of the Kr−F_t bond will lead to a decrease in the actual interactions involving an individual F_t-Kr- -F_b moiety and a decrease in the bond order. There are also fewer electrons involved in the 5c−6e bond when compared with two 3c−4e bonds, which is again consistent with a decrease in the Mayer bond order between F_b and F_t. It is useful to note that the total involvement of F_b with the two F_t atoms as measured by the Mayer bond order is 0.28, which is actually greater than that of an individual fluorine in KrF_2; this is consistent with the 5c−6e model superimposed on an ionic model in which F^- interacts with two KrF^+ cations. A similar set of results is found for XeF_2 and $Xe_2F_3^+$.[65]

The Mayer bond orders are in semiquantitative agreement with the simple valence bond descriptions of NgF^+, NgF_2, and $Ng_2F_3^+$, which predict Ng-F bond orders of one-half for NgF_2, a bond order of one for the free NgF^+ cation, a value somewhere

(61) Mayer, I. *Chem. Phys. Lett.* **1983**, *97*, 270.
(62) Mayer, I. *Theor. Chim. Acta* **1985**, *67*, 315.
(63) Mayer, I. *Int. J. Quantum Chem.* **1986**, *29*, 73.
(64) Mayer, I. *Int. J. Quantum Chem.* **1986**, *29*, 477.
(65) Dixon, D. A.; Schrobilgen, G. J. Unpublished results, also see ref 38.

Table 10. Atomic Charges, Mayer Valencies, and Mayer Bond Orders for $[KrF][MF_6]$ (M = P, As, Sb, Bi), KrF^+, $Kr_2F_3^+$, and KrF_2

	$[KrF]\cdot[PF_6]$	$[KrF][AsF_6]$	$[KrF][SbF_6]$	$[KrF][BiF_6]$	KrF^+	$Kr_2F_3^+$	KrF_2
			Atomic Charges and Valencies[a,b]				
Kr	+0.79 (1.32)	+0.80 (1.32)	+0.82 (1.31)	+0.82 (1.32)	+1.00 (1.09)	+0.85 (1.28)	+0.72 (1.35)
M	+1.16 (5.36)	+0.90 (5.60)	+1.45 (5.14)	+2.23 (3.15)			
F_t	−0.30 (0.95)	−0.27 (0.97)	−0.26 (0.98)	−0.26 (0.98)	0.00 (1.09)	−0.37 (1.04)	−0.36 (0.89)
F_b	−0.37 (0.99)	−0.31 (1.08)	−0.31 (1.08)	−0.41 (0.92)		−0.16 (1.03)	
F_a	−0.26 (1.14)	−0.20 (1.20)	−0.31 (1.08)	−0.47 (0.82)			
F_e	−0.26 (1.08)	−0.22 (1.15)	−0.32 (1.06)	−0.50 (0.76)			
F'_e	−0.24 (1.10)	−0.20 (1.18)	−0.36 (1.00)	−0.46 (0.81)			
F''_e	−0.30(1.03)	−0.27 (1.10)					
			Mayer Bond Orders[a]				
$Kr-F_t$	0.74	0.76	0.79	0.79	1.09	0.86	0.67
$Kr-F_b$	0.54	0.50	0.47	0.48		0.38	
F_b-F_t	0.19	0.18	0.17	0.18		0.14	0.22
$M-F_b$	0.23	0.37	0.42	0.18			
$M-F_a$	1.09	1.10	0.99	0.65			
$M-F_e$	1.02	1.04	0.96	0.61			
$M-F'_e$	1.03	1.05	0.90	0.55			
$M-F''_e$	0.97	0.98					

[a] Calculated values are at the LDFT level. [b] Mayer valencies are given in parentheses.

between one-half and one for the terminal Ng-F_t bonds of $Ng_2F_3^+$, and a value between zero and one-half for the Ng-F_b bonds of $Ng_2F_3^+$.

Little variation and no clear pattern is apparent among the atomic charges of the F_t-Kr- -F_b groups of the $[KrF][MF_6]$ ion pairs. The negative charges on the F_a and F_e atoms of the MF_5 groups increase on descending group 15, a trend that is consistent with a corresponding increase in fluoride ion acceptor strength (see Computational Results; Geometries. (b) KrF^+ and $[KrF][MF_6]$). Thus, the $[KrF][MF_6]$ ion pairs containing the heavier pnicogens are shown to be more ionic from their M- -F_b bond orders [0.23 (P), 0.37 (As), 0.42 (Sb), and 0.18 (Bi)], their valencies at M [5.36 (P), 5.60 (As), 5.14 (Sb), and 3.15 (Bi)], and their Kr- -F_b bond orders [0.54 (P), 0.50 (As), 0.47 (Sb), and 0.48 (Bi)]. The valencies at Kr remain nearly constant at 1.31−1.32 over the series. The $Kr-F_t$ bond orders [0.74 (P), 0.76 (As), 0.79 (Sb), and 0.79 (Bi)] and F_t- -F_b bond orders [0.19 (P), 0.18 (As), 0.17 (Sb), and 0.18 (Bi)] are intermediate with respect to those of $Kr_2F_3^+$ (0.86 and 0.14, respectively) and KrF_2 (0.67 and 0.22, respectively). The most significant increase in M- -F_b bond order and in pnicogen valence occurs on going from P to As with a smaller decrease in the Kr- -F_b bond order. Similar changes are noted for the transition from As to Sb, but no significant changes in the aforementioned parameters occur in going from Sb to Bi except that the Bi- -F_b bond order is smaller by 0.24. The anomaly seen for bismuth likely arises from the core potential used in the calculations. These results show that the degree of F^- complexation increases as the size of the central atom increases, and the coordination sphere around the pnicogen atom becomes less crowded, allowing MF_5 to more effectively compete with the KrF^+ cation for the bridge fluorine. This is consistent with the gas-phase fluoride ion affinities of PF_5, AsF_5, and SbF_5 [57] and our failure to prepare $[KrF][PF_6]$ (see Synthesis and Characterization by Raman Spectroscopy of $[Kr_2F_3][PF_6]\cdot nKrF_2$). Moreover, a comparison of the P- -F_b bond order in $[KrF][PF_6]$ with the Kr- -F_b bond order in $Kr_2F_3^+$ indicates that KrF^+ has a greater F^- affinity than PF_5. Our inability to synthesize $[KrF][PF_6]$ at low temperatures in the presence of excess PF_5 is consistent with these findings.

Conclusion

A more precise structure of KrF_2 has been obtained, and the dimorphism of KrF_2 has been confirmed by an X-ray crystal structure determination of the low-temperature α-phase. Single-crystal X-ray structure determinations and theoretical calculations show that the solid-state and gas-phase $[KrF][MF_6]$ ion pairs are strongly fluorine bridged. With the exception of theoretically predicted $KrF_2\cdot PF_5$ adduct, the $Kr-F_t$ bond length is little influenced by the MF_6^- anion. No significant difference in the Kr- -F_b bond length was observed in the AsF_6^- and SbF_6^- salts, although this bond length was found to be significantly shorter in the BiF_6^- salt, in accord with the higher covalent character associated with the weaker fluoride ion acceptor strength of BiF_5. The Raman spectra of the fluorine-bridged $[KrF][MF_6]$ ion pairs have been assigned by comparison with their calculated vibrational spectra.

The $Kr_2F_3^+$ cation is highly deformable in the solid state, specifically with regards to the Kr- -F_b bond distances and the Kr- -F_b- -Kr bridge bond angle. These deformations are attributed to long contacts between the krypton atoms in the cation and fluorine atoms associated with the anion[50] and are not reproduced by theoretical calculations of the gas-phase geometries. The calculated vibrational frequencies of $Kr_2F_3^+$ show that the prior detailed assignments[16] of the terminal symmetric and asymmetric stretching modes were incorrect and that their assignments should be interchanged.

Raman spectroscopic investigation of the KrF_2/PF_5 system indicates that the only existing species is $[Kr_2F_3][PF_6]\cdot nKrF_2$. This compound is characteristic of the $[Kr_2F_3][MF_6]\cdot nKrF_2$ (M = As, Sb, Bi) series and exhibits vibrational modes consistent with a weakly interacting $Kr_2F_3^+$ cation and an octahedral PF_6^- anion. Failure to synthesize $[KrF][PF_6]$ in the presence of excess PF_5 reflects the low fluoride ion affinity of PF_5 relative to those of the heavier pnicogen pentafluorides and conforms with the theoretical results, which predict an adduct in which PF_5 is weakly fluorine bridged to KrF_2 and the KrF_2 bond lengths exhibit little distortion from the bond lengths of free KrF_2.

Experimental Section

Caution: Anhydrous HF must be handled using appropriate protective gear with immediate access to proper treatment procedures in the event of contact with liquid HF, HF vapor, or HF solutions of krypton(II) species. Krypton(II) compounds are potent oxidizers that react explosively with water and organic materials. Extreme caution is to be exercised in their handling and disposal in order to avoid violent detonations. The recommended procedure for disposing of small quantities of KrF_2, KrF^+, and $Kr_2F_3^+$ salts in anhydrous HF solvent (ca. 200 mg of compound in 2 mL of HF or less) is by slowly pouring

the cold HF solution (0 °C or lower) into several liters of a mixture of ice and aqueous NaOH inside a properly shielded fume hood. Solution sample containers must be handled with long metal tongs and protective gloves when dumping their contents into the disposal medium.

Apparatus and Materials. Volatile materials were handled in vacuum lines constructed of stainless steel, nickel, and FEP fluoroplastic, and nonvolatile materials were handled in the dry nitrogen atmosphere of a glovebox as previously described.[66]

Arsenic pentafluoride was prepared as previously described[67] and was used without further purification. Anhydrous HF (Harshaw Chemical Co.),[68] SbF_3 (Aldrich, 98%),[66] and BiF_5 (Ozark Mahoning Co.)[17] were purified by the standard literature methods. Purified HF was stored over BiF_5 in a Kel-F vessel equipped with a Kel-F valve until used. Fluorine gas (Air Products) was used without further purification. Antimony pentafluoride was synthesized in situ by direct fluorination of SbF_3 with F_2 in anhydrous HF as previously described.[69]

(a) PF_5. Phosphorus pentafluoride (Ozark Mahoning) was purified by distillation under dynamic vacuum through two FEP traps maintained at −117 °C to remove POF_3 and HF impurities and at −196 °C to condense PF_5. This process was repeated a second time before the purified product was condensed into a prefluorinated stainless steel cylinder at −196 °C. The cylinder and contents were stored at room temperature until used.

(b) KrF_2. Krypton difluoride was prepared using a 316 stainless steel hot-wire reactor equipped with a nickel filament, similar to that originally described by Bezmel'nitsyn et al.[7] and subsequently modified and described by Kinkead et al.[9] The filament of the reactor used in the present work was fabricated from $^1/_{16}$-in. nickel rod tightly wound about a second length of $^1/_{16}$-in. rod that was, in turn, coiled and stretched into a helix. Approximately 1000 Torr (50 mmol) of krypton (Air Products, 99.995%) was initially added to the prefluorinated reactor, which was then immersed in a 20 L dewar filled with liquid nitrogen. After the reactor was cooled, 25 Torr of F_2 (Air Products, technical grade) was added, and the DC power supply for the nickel filament was adjusted to approximately 6 V and 30 A (the filament under these conditions was dull red in color), which increased the F_2 pressure to ca. 45 Torr once the temperature of the filament and reactor had stabilized. The pressure inside the hot-wire reactor was maintained between 25 and 45 Torr for each 8−12 h run. As KrF_2 formation progressed, the pressure was periodically readjusted by adding more F_2. When KrF_2 production slowed or ceased, a 1.0−2.0 mmol aliquot of krypton was condensed into the reactor. After the reaction was completed, excess fluorine was removed by pumping the reactor at −196 °C. Excess krypton and crude KrF_2 were recovered as a pink solid (because of chromium oxide fluoride contamination leached from the stainless steel reactor body) by allowing the reactor to slowly warm to room temperature while dynamically pumping the volatile contents through a $^1/_2$-in. o.d. FEP U-trap that was cooled to −196 °C. The Kr/KrF_2 mixture was then warmed and dynamically pumped at −78 °C to remove unreacted krypton. The crude KrF_2 was purified by briefly warming the sample to approximately 0 °C and flash distilling off the more volatile chromium oxide fluorides. The remaining colorless KrF_2 was finally warmed to room temperature and rapidly sublimed into a $^3/_8$-in. o.d. FEP tube equipped with a Kel-F valve and stored under nitrogen or argon at −78 °C until used. This synthesis is highly reproducible and typically yields 2.5−3.0 g of purified KrF_2 over a 12 h period.

***β*-[KrF][AsF_6] and [Kr_2F_3][AsF_6]·[KrF][AsF_6].** The salts [Kr_2F_3][AsF_6]·[KrF][AsF_6] and [KrF][AsF_6] were prepared in a manner similar to that described earlier for [KrF][AsF_6].[16] Approximately 100 mg of KrF_2 was condensed at −196 °C into a $^1/_4$-in. o.d. T-shaped FEP reactor equipped with a stainless steel valve. An excess of AsF_5 was then condensed on top of the KrF_2, and the reaction vessel was cycled between −78 and −53 °C with agitation for 1 h. Excess AsF_5 was then removed under dynamic vacuum at −78 °C. Raman spectroscopy at −78 °C confirmed the presence of both α-[KrF][AsF_6] and *β*-[KrF][AsF_6] in the sample.[16] The [Kr_2F_3][AsF_6]·[KrF][AsF_6] adduct was synthesized by condensing a slight stoichiometric excess of KrF_2 onto a sample of [KrF][AsF_6]. Sufficient anhydrous HF (ca. 1.5 mL) was condensed into each reactor until the sample was completely soluble at −10 °C. The reactor was then backfilled with ultra-high-purity (UHP) nitrogen (99.999%, <10 ppm O_2 + CO + CO_2 + H_2O) or argon (99.999%, <2 ppm O_2, <3 ppm H_2O) and stored at −78 °C.

[KrF][SbF_6] and [KrF][BiF_6]. The salts, [KrF][SbF_6] and [KrF][BiF_6], were prepared by the literature methods.[16,17] In each preparation, approximately 100 mg of the pentafluoride was dissolved in 1−2 mL of anhydrous HF in a rigorously dried and prefluorinated T-shaped reaction vessel fabricated from $^1/_4$-in. o.d. FEP tubing and fitted with a stainless steel valve. A stoichiometric excess of KrF_2 (ca. 10% to account for the passivation of the stainless steel valve by KrF_2) was then condensed on top of the mixture at −196 °C before being warmed to −78 °C and backfilling the vessel with UHP nitrogen or argon. The vessel was then carefully warmed to 0 °C and agitated for 10 min before storing at −78 °C.

[Kr_2F_3][PF_6]·*n*KrF_2. Approximately 100 mg of KrF_2 was vacuum-distilled into a dried and F_2-passivated FEP reaction vessel equipped with a stainless steel valve. Phosphorus pentafluoride (bp, −75 °C) was then condensed into the reaction vessel and allowed to react at −78 °C. The reaction was monitored biweekly by Raman spectroscopy, and additional aliquots of PF_5 were added as necessary. The reaction was determined to be complete when the changes in the Raman spectrum ceased after 7 weeks, and the intense $\nu_1(\Sigma^+_g)$ vibration of KrF_2 was barely visible at 465 cm^{-1}. Further reaction with PF_5 failed to produce [Kr_2F_3][PF_6] or [KrF][PF_6]. The spectrum was also monitored for [O_2][PF_6] arising from the reaction of $Kr_2F_3^+$ with O_2 or H_2O. Only extremely weak peaks associated with the O_2^+ stretches at 1859.5 and 1863.0 cm^{-1} were observed after 7 weeks.

[Kr_2F_3][SbF_6]·KrF_2 and [Kr_2F_3]$_2$[SbF_6]$_2$·KrF_2. The [Kr_2F_3][SbF_6]·KrF_2 and [Kr_2F_3]$_2$[SbF_6]$_2$·KrF_2 salts were synthesized in the same fashion as the [KrF][SbF_6] salt with only minor modifications. The [Kr_2F_3][SbF_6]·KrF_2 salt was synthesized using a large excess of KrF_2 ($3.5KrF_2$:SbF_5, a 75 mol % excess with respect to $Kr_2F_3^+$). The [Kr_2F_3]$_2$[SbF_6]$_2$·KrF_2 salt was synthesized using a 0.6 mol % stoichiometric excess of KrF_2. After both samples were crystallized, both [Kr_2F_3]$_2$[SbF_6]$_2$·KrF_2 and [KrF][SbF_6] were shown to be present by determinations of their respective unit cell parameters.

Crystal Growth. α-KrF_2. Approximately 50 mg of KrF_2 was distilled into one arm of an h-shaped reaction vessel constructed of FEP and equipped with a Kel-F valve. The reaction vessel was evacuated at −78 °C on a metal vacuum line and then allowed to stand under static vacuum. The arm containing KrF_2 was warmed from −78 to −40 °C using a dry ice/acetone bath, while the other arm of the reactor was maintained at −78 °C. Over the course of several hours, nearly cubic crystals of KrF_2 were deposited in the colder arm above the coolant level. The reactor was backfilled with UHP N_2 when the sublimation was complete and stored at −78 °C until the crystals could be mounted on the X-ray diffractometer.

[KrF][MF_6] (M = As, Sb, Bi), [Kr_2F_3]$_2$[MF_6]$_2$·KrF_2, and [Kr_2F_3][MF_6]·KrF_2 (M = As, Sb). The $Kr_2F_3^+$ salts and their adducts with KrF_2 were completely dissolved, or nearly completely in the case of the moderately soluble [KrF][BiF_6] salt, by carefully warming the solutions to a maximum of −10 °C to minimize decomposition. The reaction vessel was then slowly cooled by insertion into a glass, vacuum-jacketed tube that was cooled by a flow of cold nitrogen gas. The rate of cooling was controlled by the nitrogen gas flow rate and could be regulated (±0.2 °C) between room temperature and −90 °C. Once cooled to −80 °C, the bulk of the HF was decanted into the sidearm of the T-shaped FEP reactor, which was cooled to −196 °C immediately before the solvent was decanted. The sample was then pumped on dynamically to thoroughly dry the crystals before the sidearm was heat sealed off. The reactor was then backfilled with dry N_2 and stored at −78 °C until the crystals could be mounted on the X-ray diffractometer. The [KrF][MF_6] (M = As, Sb, Bi) salts all

(66) Casteel, W. J., Jr.; Kolb, P.; LeBlond, N.; Mercier, H. P. A.; Schrobilgen, G. J. *Inorg. Chem.* **1996**, *35*, 929.
(67) Mercier, H. P. A.; Sanders, J. C. P.; Schrobilgen, G. J.; Tsai, S. S. *Inorg. Chem.* **1993**, *32*, 386.
(68) Emara, A. A. A.; Schrobilgen, G. J. *Inorg. Chem.* **1992**, *31*, 1323.
(69) LeBlond, N.; Dixon, D. A.; Schrobilgen, G. J. *Inorg. Chem.* **2000**, *39*, 2473.

crystallized as discreet colorless needles, while $[Kr_2F_3][SbF_6]\cdot KrF_2$ and $[Kr_2F_3]_2[SbF_6]_2\cdot KrF_2$ crystallized as intergrown pale yellow plates.

Raman Spectroscopy. Raman spectra of $[Kr_2F_3][PF_6]\cdot nKrF_2$ were recorded as previously described.[66] The spectra were recorded in a $^1/_4$-in. FEP sample tube under 1000 Torr of PF_5 at −80 C° using the macrochamber of the instrument. The 514.5-nm line of an Ar^+ laser with an output setting of 300 mW was used for excitation of the sample with a laser spot of ∼1 mm at the sample. The slit width settings corresponded to a resolution of 1 cm^{-1}. A total of 10 reads each having 60 s integration times were summed using a CCD detector.

X-ray Crystallography. Crystal Mounting and the Collection of X-ray Data. All crystals were mounted at −110±5 °C as previously described,[70] and data were collected at −113 to −130 °C. All crystals were centered on a P4 Siemens diffractometer, equipped with a Siemens SMART 1K CCD area detector, controlled by SMART,[71] and a rotating anode emitting Kα radiation monochromated (λ = 0.710 73 Å) by a graphite crystal. The crystal to detector distance was typically 5 cm, and the data collection was carried out in a 512 × 512 pixel mode using 2 × 2 pixel binning. Processing of the raw data was completed using SAINT+,[72] which applied Lorentz and polarization corrections to the three-dimensionally integrated diffraction spots. Scaling of the integrated data was completed with SADABS,[73] which applies decay corrections, and an empirical absorption correction on the basis of the intensity ratios of redundant reflections.

Solution and Refinement of the Structures. The program XPREP[74] was used to confirm the unit cell dimensions and the crystal lattice. A solution was found using direct methods to determine the locations of the heavy elements (Kr, As, Sb, Bi). The fluorine positions were identified in successive difference Fourier syntheses. Final refinements were obtained using data that had been corrected for absorption by introducing an extinction coefficient and optimized using anisotropic thermal parameters.

Calculations. Electron structure calculations at the DFT level were done with the density-functional theory[75] program DGauss[76−78] on SGI computer systems. The DZVP basis set[79] was used for all atoms, except for Bi where the Hay-Wadt ECP basis set was used[80−82] with the fitting sets in UniChem.[83] All calculations were done at the local level with the potential fit of Vosko, Wilk, and Nusair.[84] The geometries were optimized by using analytic gradient methods, and second derivatives were also calculated analytically.[85] The HF calculations were done with the program Gaussian-98.[86] For the F and P atoms, the polarized double-ζ basis sets of Dunning and Hay were used.[87] For the remaining atoms, the effective core potentials and double-ζ basis sets of Hay and Wadt[80−82] were used with the polarization functions of Huzinaga et al.[88]

Acknowledgment. We thank the donors of the Petroleum Research Fund, administered by the American Chemical Society, for support of this work under ACS-PRF 33594-AC3. We also thank the Natural Sciences and Engineering Research Council of Canada for a postgraduate scholarship and McMaster University for a Dalley Fellowship to J.F.L. and the Canada Council for the award of a Killam Research Fellowship (1998 and 1999) to G.J.S. The density-functional theory calculations were performed in the William R. Wiley Environmental Molecular Sciences Laboratory funded by the Office of Biological Environmental Research, U.S. Department of Energy, under Contract DE-AC06-76RLO 1830 with the Battelle Memorial Institute, which operates the Pacific Northwest National Laboratory, a multiprogram national laboratory for the Department of Energy.

Supporting Information Available: An X-ray crystallographic file, in CIF format, for the structure determinations of α-KrF_2, $[KrF][MF_6]$ (M = As, Sb, Bi), $[Kr_2F_3][SbF_6]\cdot KrF_2$, $[Kr_2F_3]_2[SbF_6]_2\cdot KrF_2$, and $[Kr_2F_3][AsF_6]\cdot[KrF][MF_6]$. This material is available free of charge via the Internet at http://pubs.acs.org.

IC001167W

(70) Gerken, M.; Dixon, D. A.; Schrobilgen, G. J. *Inorg. Chem.* **2000**, *39*, 4244.
(71) *SMART*, Version 5.054; Siemens Energy and Automation Inc.: Madison, WI, 1999.
(72) *SAINT+*, Version 6.01; Siemens Energy and Automation Inc.: Madison, WI, 1999.
(73) Sheldrick, G. M. SADABS (Siemens Area Detector Absorption Corrections), Personal Communication, 1998.
(74) Sheldrick, G. M. *SHELXTL*, Version 5.1; Siemens Analytical X-ray Instruments Inc.: 1998.
(75) Par, R. G.; Yang, W. *Density-Functional Theory of Atoms and Molecules*; Oxford University Press: New York, 1989.
(76) Andzelm, J.; Wimmer, E.; Salahub, D. R. In *The Challenge of d and f Electrons: Theory and Computation*; Salahub, D. R., Zerner, M. C., Eds.; ACS Symposium Series 394; American Chemical Society: Washington, DC, 1989; p 228.
(77) Andzelm, J. In *Density Functional Theory in Chemistry*; Labanowski, J., Andzelm, J., Eds.; Springer-Verlag: New York, 1991; p 155.
(78) Andzelm, J. W.; Wimmer, E. J. *J. Chem. Phys.* **1992**, *96*, 1280. DGauss is a density-functional program that is part of UniChem and is available from Oxford Molecular. Versions 4.1 and 5.0 were used.
(79) Godbout, N.; Salahub, D. R.; Andzelm, J.; Wimmer, E. *Can. J. Chem.* **1992**, *70*, 560.
(80) Hay, P. J.; Wadt, W. R. *J. Chem. Phys.* **1982**, *82*, 271.
(81) Hay, P. J.; Wadt, W. R. *J. Chem. Phys.* **1982**, *82*, 285.
(82) Hay, P. J.; Wadt, W. R. *J. Chem. Phys.* **1982**, *82*, 299.
(83) Lee, C.; Chen, H. Unpublished results; see *UniChem Manual*, *Version 3.0*.
(84) Vosko, S. J.; Wilk, L.; Nusair, W. *Can. J. Phys.* **1980**, *58*, 1200.
(85) Komornicki, A.; Fitzgerald, G. J. *J. Chem. Phys.* **1993**, *98*, 1398.
(86) Frisch, M. J.; Trucks, G. W.; Schlegel, H. B.; Scuseria, G. E.; Robb, M. A.; Cheeseman, J. R.; Zakrzewski, V. G.; Montgomery J. A., Jr.; Stratmann, R. E.; Burant, J. C.; Dapprich, S.; Millam, J. M.; Daniels, A. D.; Kudin, K. N.; Strain, M. C.; Farkas, O.; Tomasi, J.; Barone, V.; Cossi, M.; Cammi, R.; Mennucci, B.; Pomelli, C.; Adamo, C.; Clifford, S.; Ochterski, J.; Petersson, G. A.; Ayala, P. Y.; Cui, Q.; Morokuma K.; Malick D. K.; Rabuck A. D.; Raghavachari, K.; Foresman, J. B.; Ciosloski, J.; Ortiz, J. V.; Stefanov, B. B.; Lui, G.; Liashenko, A.; Piskorz, P.; Komaromi, I.; Gomperts, R.; Martin, R. L.; Fox, D. J.; Keith T.; Al-Laham, M. A.; Peng, C. Y.; Nanayakkara, A.; Gonzalez, C.; Challacombe, M.; Gill, P. M. W.; Johnson, B.; Chen, W.; Wong, M. W.; Andres, J. L.; Gonzalez, C.; Head-Gordon, M.; Replogle, E. S.; Pople, J. A. *Gaussian 98*, revision A.4; Gaussian, Inc.: Pittsburgh, PA, 1998.
(87) Dunning, T. H., Jr.; Hay, P. J. In *Methods of Electronic Structure Theory*; Schaefer, H. F., III, Ed.; Plenum: New York, 1977; p 1.
(88) Huzinaga, S.; Andzelm, J.; Klobukowski, M.; Radzio-Andzelm, E.; Sakai, Y.; Tatwaki, H. *Gaussian Basis Sets for Molecular Calculations*; Physical Sciences Data 16; Elsevier: Amsterdam, 1984.